QUANTIFYING THE IMMEDIATE CARBON EMISSIONS FROM EL NIÑO-MEDIATED WILDFIRES IN HUMID TROPICAL FORESTS

Kieran Daniel Withey

Lancaster Environment Centre

University of Lancaster

This dissertation is submitted for the degree of Master of Science by Research

March 2019

Quantifying the immediate carbon emissions from El Niño-mediated wildfires in humid tropical forests – Kieran Withey, November 2018

Quantifying the immediate carbon emissions from El Niño-mediated wildfires in humid tropical forests – Kieran Withey, November 2018

DECLARATION

This thesis has not been submitted in support of an application for another degree at this or any other university. It is the result of my own work and includes nothing that is the outcome of work done in collaboration except where specifically indicated. Many of the ideas in this thesis were the product of discussion with my supervisors: Jos Barlow and Fernando Espírito-Santo.

The field data use herein were not collected by myself, they was collected over a number of years as part of several NERC-funded projects, and their collection was coordinated by Erika Berenguer.

Excerpts of this thesis have been published in the following academic publication:

Withey, K. *et al.* (2018) 'Quantifying immediate carbon emissions from El Niño-mediated wildfires in humid tropical forests', *Philosophical Transactions of the Royal Society B: Biological Sciences*, 373(1760), p. 20170312. doi: 10.1098/rstb.2017.0312.

Kieran Daniel Withey, BSc

Lancaster University, UK

Quantifying the immediate carbon emissions from El Niño-mediated wildfires in humid tropical forests – Kieran Withey, November 2018

Quantifying the immediate carbon emissions from El Niño-mediated wildfires in humid tropical forests – Kieran Withey, November 2018

Quantifying the immediate carbon emissions from El Niño-mediated wildfires in humid tropical forests – Kieran Withey, November 2018

Quantifying the immediate carbon emissions from El Niño-mediated wildfires in humid tropical forests – Kieran Withey, November 2018

ABSTRACT

Wildfires produce substantial CO_2 emissions in the humid tropics during El Niño-mediated extreme droughts, and these emissions are expected to increase in coming decades. Immediate carbon emissions from uncontrolled wildfires in human-modified tropical forests can be considerable owing to high necromass fuel loads. Yet, data on necromass combustion during wildfires are severely lacking. The present study evaluated necromass carbon stocks before and after the 2015–2016 El Niño in Amazonian forests distributed along a gradient of prior human disturbance. Landsat-derived burn scars were used to extrapolate regional immediate wildfire CO_2 emissions during the 2015–2016 El Niño. Before the El Niño, necromass stocks varied significantly with respect to prior disturbance and were largest in undisturbed primary forests (30.2 ± 2.1 Mg ha^{-1}, mean $\pm$ s.e.) and smallest in secondary forests (15.6 ± 3.0 Mg ha^{-1}). However, neither prior disturbance nor a proxy of fire intensity (median char height) explained necromass losses due to wildfires. In the 6.5 million hectare (6.5 Mha) study region, almost 1 Mha of primary (disturbed and undisturbed) and 20,000 ha of secondary forest burned during the 2015–2016 El Niño. Covering less than 0.2% of Brazilian Amazonia, these wildfires resulted in expected immediate CO_2 emissions of approximately 30 Tg, three to four times greater than comparable estimates from global fire emissions databases. Uncontrolled understorey wildfires in humid tropical forests during extreme droughts are a large and poorly quantified source of CO_2 emissions.

Quantifying the immediate carbon emissions from El Niño-mediated wildfires in humid tropical forests – Kieran Withey, November 2018

ACKNOWLEDGEMENTS

x

CONTENTS

LIST OF TABLES

LIST OF FIGURES

LIST OF ABBREVIATIONS AND ACRONYMS

AGB = Aboveground Biomass

AGLB = Aboveground Live Biomass

CO_2 = Carbon dioxide

ENSO = El Niño – Southern Oscillation

AMO = Atlantic

DBH = Diameter at Breast Height

CWD = Coarse Woody Debris

FWD = Fine Woody Debris

ha = hectare

LIST OF APPENDICES

1 INTRODUCTION

1.1 Background

There is widespread consensus among the scientific community that climate change is already underway and will result in changes to the Earth system that will pose significant challenges to societies across the globe (Crowley, 2000; Pachauri et al., 2014). Contemporary climate change is principally the result of anthropogenically driven changes in climate forcing agents, with increases in atmospheric concentrations of greenhouse gases (GHGs), such as carbon-dioxide (CO_2) and methane (CH_4) being responsible for the largest increases in positive forcing (Hansen & Sato, 2001; Pachauri et al., 2014). Atmospheric concentrations of CO_2 are currently the highest they have been for over 800,000 years (Lüthi et al., 2008) and the iconic level of 400 ppm of CO_2 was first exceeded in May 2013 (Le Quéré et al., 2016). This is a >40% increase from the 277 ppm estimated for the start of the industrial era (*c.* 1750 A.D.) (Joos & Spahni, 2008).

Observed changes in contemporary climate due to increases in GHGs are expected to continue to impact profoundly natural and human systems (Crowley, 2000; Thornton et al., 2014). For example, the global mean temperature rose by 0.85°C during the period from 1880 to 2012 (Pachauri et al., 2014). Furthermore, 1983–2012 was likely the warmest 30-year period in the northern hemisphere for at least the last 1,400 years. In addition, the period from 1901 to 2010 saw

precipitation increase over mid-latitude areas of the northern hemisphere and global mean sea level rose by 0.19 m (Pachauri et al., 2014). Future climate change scenarios suggest a further substantial warming of 0.3–0.7°C for the coming decades (2016–2035) and a warming of 0.3–4.8°C for the end of the 21st century (2081–2100), relative to the 1986–2005 global mean (Pachauri et al., 2014). Projections of future precipitation patterns are more heterogenous across the globe. In general, mid-latitude wet regions will very likely see increases in precipitation, while decreases are likely in many mid-latitude and subtropical dry regions (Pachauri et al., 2014). Wet tropical regions will very likely see increases in the intensity and frequency of extreme precipitation events (i.e. droughts and floods) (Pachauri et al., 2014). The severity of changes to the Earth's climate system will depend to a great extent on the future behaviour of different components of the Earth system, such as the carbon cycle.

The global carbon cycle has played a fundamental role in ameliorating the effects of past and current anthropogenic emissions of CO_2 (Ciais et al., 2013; Keenan et al., 2016). Atmospheric concentrations of CO_2 are currently growing more slowly than anthropogenic emissions, due to the compensatory effects from within the global carbon cycle. There has been a strengthening of the global (land and ocean) carbon sink over the past five decades and this is estimated to absorb *c.* 50% of anthropogenic CO_2 emissions (Ballantyne et al., 2012; Barlow et al., 2015). Nonetheless, the sign and strength of carbon uptake across the globe is poorly quantified and understood, leading to one of the largest sources of uncertainty in future climate predictions (Le Quéré et al., 2016).

Tropical forests play a key role in the carbon cycle and have been considered a net CO_2 sink, helping to reduce the atmospheric concentration of CO_2 (Houghton, Baccini, & Walker, 2018). The future strength and sign of this critical component of the carbon cycle is unclear (Mitchard, 2018) and the CO_2-fertilisation effect may be reaching a physiological ceiling in tropical forests due to contemporary climatic conditions (Brienen et al., 2015; Liu et al., 2017). For example, droughts in tropical forests—such as those seen during El Niño–Southern Oscillation events—have been responsible for turning this important sink into a

source of CO_2 (e.g. Phillips et al. 2009; Lewis et al. 2005; Baccini et al. 2017; Gatti et al. 2014; Cox et al. 2013; Yang et al. 2018). Furthermore, Brienen et al. (2015) have reported a long-term decline in the Amazon carbon sink, suggesting we may be approaching a tipping point (Malhi et al., 2009; Nepstad et al., 2008; Nobre & Borma, 2009).

Correlation between measurements of atmospheric CO_2 concentrations and tropical temperatures suggested that one of the strongest sources of interannual variability of CO_2 is El Niño—Southern Oscillation (ENSO) (Jones et al., 2001; Wang et al., 2013), with much of this variability being attributed to tropical forests (Wang et al. 2013). ENSO is an atmospheric and oceanographic phenomenon originating in the tropical latitudes of the Pacific Ocean which has been present in the Earth system for at least the past 130,000 years (Tudhope et al., 2001) and has been strengthening for at least 200 years (Schöngart et al., 2004), with further increases in its strength predicted (Cai et al., 2014; Timmermann et al., 1999). El Niño—the positive up cycle of ENSO—sees a pool of warm surface water migrate east from the western Pacific to the central and eastern Pacific, which results in the disturbance of the Walker circulation and global atmospheric circulation, ultimately leading to a warming and increases in dry season length across much of the humid lowland tropics (Malhi et al., 2018), including across the Amazon (Marengo & Espinoza, 2016)

1.2 Study system / focus

The Amazon forest is the world's largest tropical rainforest, playing a multifaceted role in the Earth system. It holds ≥86 Pg C, or *c.* 40% of the biomass held in tropical forests globally (Malhi et al., 2006; Saatchi et al., 2011; Saatchi et al., 2007). Beyond simply storing a vast amount of carbon, Amazonian forests are the most species-rich ecosystems on the globe (Hoorn et al., 2010). The tree flora alone harbours *c.* 16,000 species—or 30–50% of all tropical tree species (Slik et al., 2015). The Amazon is also home to a diversity of human cultures and societies (Little, 2005; Roosevelt, 2013). The ecosystem services offered by Amazonian forests—such as water cycling, food production, and the provision of raw materials—benefit societies, both locally and globally (Boers et al., 2017; Khanna et al., 2017; Kunert et al., 2017; Strand et al., 2018). Moreover, the Amazon currently serves as a carbon sink, helping to remove and store part of the anthropogenically released CO_2 emissions (Pan et al., 2011).

Despite its local, regional, and global importance, the Amazon has faced numerous threats, which have been on the increase in recent decades (Davidson et al., 2012). Deforestation, resulting in the most part from agricultural expansion, is the most recognisable risk to the Amazon's biodiversity and ecosystem services (Ferreira et al., 2012; Spracklen & Garcia-Carreras, 2015). Conversion of forest for other land-uses is responsible for a myriad of negative impacts on biodiversity, ecosystem properties, and global climate (Davidson et al., 2012; Spracklen & Garcia-Carreras, 2015). Deforestation rates declined 76% from 2004 to 2017, decreasing from nearly 28,000 km^2 y^{-1} in 2004 to less than 7,000 km^2 y^{-1} in 2017, which is widely thought to be a result of concerted efforts from governmental and non-governmental agencies (Aragão et al., 2018).

While there have been consistent reductions in deforestation/clear-cutting over the past decade, these have not been sufficient to preserve forest

quality as more cryptic human-induced disturbances have emerged, such as selective-logging, hunting, and wildfires, that are often much harder to detect at larger spatial scales (Peres et al., 2006; Barlow et al. 2016) and have significant ecological impacts while maintaining certain forest attributes (Ghazoul & Chazdon, 2017). These human-modified forests—forests that have been structurally altered by anthropogenic disturbance, such as selective logging and fires, and those regenerating following deforestation (commonly called *secondary forests*)—then become more susceptible to wildfires in the future and large-scale understorey wildfires, which were unprecedented in recent millennia (Bush et al., 2007; Kauffman & Uhl, 1990; Turcq et al., 1998), are being seen with increased frequencies (Aragão et al., 2018).

Although droughts have been recorded in the Amazon for millennia, fires are unlikely to have been regular occurrences, with return intervals on the order of centuries or millennia since the end of the last ice-age (McMichael et al., 2012; Power et al., 2008). Forest fires in humid tropical forest such as the Amazon can start naturally by means of lightning strikes, but lightning strikes are generally followed by rainfall; thus such fires would likely have been short-lived and would have affected only very small areas of the Amazon (Pivello, 2011). Anthropogenic ignitions are by far the most common proximate cause of forest fires in Amazonia. During pre-Colombian times, indigenous peoples would carry out prescribed burns as part of shifting cultivation practices, only after strict planning in accordance with land-use histories and weather conditions (Pivello, 2011).

Pervasive human modification of tropical forest landscapes, through, for example, road building, cattle ranching and timber exploitation, combined with severe drought events and the widespread use of fire as a land management tool, has fundamentally altered Amazonian fire regimes. Uncontrolled large-scale wildfires have become increasingly common over recent decades (Jolly et al., 2015) and are witnessed with sub-decadal frequency (Chen et al., 2011). Such wildfires result in high rates of tree mortality (Barlow and Peres 2004; Brando et al. 2016), shifts in forest structure (Barlow and Peres 2004; Brando et al. 2016) and drier microclimatic conditions (Cochrane & Schulze, 1999), ultimately leading

to increased susceptibility to future wildfires (Alencar et al., 2011; Cochrane et al., 1999; Cochrane & Schulze, 1999). The CO_2 emissions from such wildfires are expected to grow further (Aragão et al., 2018), as fire-conducive weather patterns—such as increasing temperatures and more intense droughts—increase across the humid tropics, particularly in South America (Jolly et al., 2015).

Carbon emissions from understorey wildfires can be split into committed and immediate emissions. Committed emissions result from the complex interplay between delayed tree mortality and decomposition, and are dependent on future climatic conditions and human influences (Goetz et al., 2015). Recent research has shown that the long-term storage of carbon in wildfire-affected Amazonian forests can be compromised for decades: even 31 years after a wildfire event, burned forests store approximately 25% less carbon than unburned control sites due to high levels of tree mortality that are not compensated by regrowth (Silva et al., 2018). Immediate emissions are those that occur during wildfires and, in contrast to committed emissions, are relatively simple to estimate. Biome- and continent-wide analyses that rely on satellite observations (known as top-down studies) suggest that these immediate emissions from tropical forests can be substantial (Liu et al., 2017; van der Laan-Luijkx et al., 2015), and, for example, can transform the Amazon basin from a carbon sink to a large carbon source during drought years (Gatti et al., 2014).One potentially important source of immediate carbon emissions during wildfires is the dead organic matter found on forest floors. This necromass, which includes leaf litter and woody debris, is a fundamental component of forest structure and dynamics and can account for up to 40% of the carbon stored in humid tropical forests (Chao et al., 2009; Palace et al., 2012; Pan et al., 2011). During long periods of drought, this large carbon pool can become highly flammable (Ray, Nepstad, & Moutinho, 2005).

1.3 Knowledge gaps

Several on-the-ground studies have quantified the necromass stocks across a relatively wide area of Amazonia. However, these studies have overwhelmingly focused on undisturbed primary forests (Chao et al., 2009); studies that estimate necromass in human-modified tropical forests across Amazonia are rare (c.f. Keller et al. 2004; Palace et al. 2007). This represents a key knowledge gap limiting our understanding of necromass fuel loads across human-modified Amazonian forests, which are increasingly common (Keenan et al. 2015) and are more vulnerable to wildfires (Alencar et al., 2006; Cochrane, 2003; Uhl & Kauffman, 1990). In addition, relatively fewer local-scale, bottom-up studies have quantified combustion characteristics in humid tropical forests following fires, and those which have been carried out have followed fires related to deforestation and slash-and-burn practices (see van Leeuwen et al. 2014 for a recent review). To date, no study has quantified fuel combustion characteristics after uncontrolled wildfires using before and after measurements in Amazonia. These knowledge gaps and data shortfalls limit our understanding of the immediate carbon emissions from understorey wildfires. Improving such estimates is essential for refining Earth Systems models and both national and global estimates of greenhouse gas emissions.

1.4 Project aims

The immediate CO_2 emissions from wildfires across an almost 1-million-hectare region of eastern Amazonia (Figure 1) that experienced extreme drought conditions during the 2015–16 El Niño (Jiménez-Muñoz et al., 2016) are quantified using a hybrid bottom-up/top-down approach. Data were combined from a previously published large-scale field assessment of carbon stocks (Berenguer et al., 2014) with on-the-ground measurements of woody debris before and after the 2015–2016 El Niño, proxies of fire intensity and coverage within study plots, and remotely sensed analyses of fire extent across the region. More specifically, the following objectives are addressed: (a) quantify carbon stocks vulnerable to combustion across human-modified tropical forests in central-eastern Amazonia, (b) use post-burn measurements to investigate the factors influencing the loss of necromass during wildfires, (c) estimate region-wide immediate carbon emissions from wildfires, and (d) compare these region-wide emission estimates with those derived from widely used global fire emissions databases.

Kieran Daniel Withey - March 2019

2 METHODS

2.1 Study region

This study focuses on a ~6.5 million ha region of central-eastern Amazonia close to the convergence of the Tapajós and Amazon rivers in Pará state, Brazil (Figure 4). This region harbours tropical moist broadleaf forest, which is mainly composed of dense evergreen *terra firme* vegetation and to a much lesser extent, deciduous vegetation (Costa et al., 2010). The native undisturbed forest has a closed canopy with tree heights up to 55 m (Pan, Birdsey, Phillips, & Jackson, 2013). The climate is seasonal with mean annual temperatures of 25°C and a dry season (August–November) with annual precipitation of 1,920 mm and slightly higher temperatures than the wet season (December–July) (Costa et al., 2010; INMET, 2018). Average precipitation in the driest months is 100 mm per month, yet this is rarely below the annual mean evapotranspiration (3.4 mm d^{-1}) (Costa *et al.*, 2010; INMET 2018). Soils are predominantly nutrient-poor clay-rich oxisols (*c.* 60% clay) with some sandy utisols (Rice et al., 2004).

2.2 Estimation of necromass carbon stocks

In 2010, 107 plots (0.25 ha) were established in a human-modified region of central-eastern Amazonia. Plots were located in the municipalities of Santarém, Belterra, and Mojuí dos Campos in the state of Pará, Brazil, and form part of the Sustainable Amazon Network (*RAS—Rede Amazônia Sustentável* in Portuguese (Gardner et al., 2013)). Study plots covered a range of prior human impacts and included undisturbed primary forests (n = 17), primary forests selectively logged prior to 2010 (n = 26), primary forests burned prior to 2010 (n = 7), primary forests logged and burned prior to 2010 (n = 24), and secondary forests that have become established following complete removal of vegetation (n = 33; see Table 1).

Table 1. Forest classifications for pre-El Niño forest disturbance classes and the number of plots sampled in 2010, 2014-15 and 2017. The 2015-16 sample occurred after the extensive wildfires and is a subset of the 2014-15 sample.

Pre-El Niño forest class	Definition	Necromass assessment (2010)	Monitoring of coarse woody debris (2014-2016)	Fire intensity and plot burned area (2017)
Undisturbed primary forest	Primary forest with no evidence of human disturbance, such as fire scars or standing tree damage	17	5	5
Logged primary forest	Primary forest with evidence of logging, such as logging debris	26	5	5
Burned primary forest	Primary forest with evidence of recent fire,	7	0	0

	such as fire scars			
Logged-and-burned primary forest	Primary forest with evidence of both logging and fire	24	4	5
Secondary forest	Forest regenerating after complete removal of native vegetation	33	4	2

Summary carbon estimates for aboveground live biomass, dead wood, litter, and soil for these 107 plots can be found in Berenguer et al. (2014). Here, four components of necromass stocks were estimated: standing-dead tree and palm stems, coarse woody debris (CWD; ≥ 10 cm diameter at one extremity), fine woody debris (FWD; 2-10 cm diameter at both extremities), and leaf litter (including twigs < 2 cm diameter at both extremities, leaves, and fruits and seeds). Once biomass estimates were obtained for each necromass component they were then standardised to per unit area (hectare), and the carbon content was assumed to be 50% of biomass dry weight (Eggleston et al., 2006)

2.2.1 Standing-dead stems

To estimate the necromass stocks of standing-dead stems (trees and palms), first the diameter and height of all large (≥10cm DBH) dead-standing trees and palms were measured in each plot (0.25 ha). The diameter and height of all small (≥2–10cm DBH) dead-standing trees and palms were estimated in five subplots of 5 x 20 m in each plot.

Second, the allometric equations of Hughes, Kauffman, and Jaramillo (1999) were used to estimate biomass (B) of small and large standing-dead tree

stems. The (B) biomass of large (≥10 cm DBH) dead standing trees was estimated using:

(Eq. 1) $$B = 0.42\pi H (D/2)^2$$

where H is tree height in metres a D is DBH in centimetres.

While small standing-dead trees (< 10 cm DBH) were estimated using the following equation:

(Eq. 2) $$B = \mathrm{CF} \times 10^{-6}(\exp(4.6014 + 1.1204\ln(D^2)))$$

where D is DBH in centimetres and CF is a correction factor to reduce the bias caused by conversion from logarithmic to arithmetic units. The CF value for small tree stems is 1.14 (see Hughes, Kauffman, and Jaramillo 1999 for further details).

Third, the allometric equations of Cummings et al. (2002) were used to estimate the biomass (B) of standing-dead palms. Large palm stems (≥10 cm) were estimated using the following equation:

(Eq. 3) $$B = H\pi r^2 \times 10^{-6}\mathrm{Sg}$$

where H is palm height in metres, Sg is specific wood gravity (g cm^{-3}), and r is the stem's radius.

While small standing-dead palms (<10 cm) were estimated using the following equation:

(Eq. 4)
$$B = 1.0931 \times 10^{-6}(\exp(1.321) \times \ln(D^2) + 3.2758)$$

where D is DBH in cm.

2.2.2 Woody Debris

The five (5 m × 20 m) subplots were also used to estimate the diameters and lengths of all pieces of fallen CWD (≥10 cm). To estimate the biomass of each piece of CWD, Smalian's formula (Chao et al., 2009) was first used to estimate its volume:

(Eq. 5)
$$V = L_{cwd}\left[\frac{\pi(D_1/2)^2 + \pi(D_2/2)^2}{2}\right]$$

where L_{cwd} (m) is the length of the CWD and D_i, $i \in 1,2$, is the diameter (m) at either extremity.

Next, the biomass of each piece of CWD was estimated using its decomposition class which was estimated in the field using the five-point scale and biomass density values of Keller et al., (2004). To avoid overestimation, the percentage of void space in each piece of CWD (i.e. the percentage of the idealised shape that was missing due to damage/void space from decomposition) was estimated visually in the field and discounted from each piece.

To assess FWD stocks, five subplots (2 m × 5 m) were established in each of the 107 study plots. All FWD was collected from the subplots and weighed in the field. A subsample (≤1 kg) from each subplot was oven-dried to a constant weight. The wet-to-dry ratios of the FWD samples were used to estimate the total FWD stocks per plot.

2.2.3 Leaf Litter

To estimate the biomass of leaf litter, ten 0.5 m × 0.5 m quadrats were established in each of the 107 study plots and all leaf litter was removed down to the soil organic layer. Leaf litter was oven-dried to constant weight to obtain an estimate of leaf litter stocks.

2.3 Data analysis of field-based estimates

Kruskal-Wallis and Conover-Iman tests with Bonferroni adjustments were used to investigate the variations in carbon stocks stored in each necromass component (i.e., dead-standing stems, CWD, FWD, and leaf litter) from the 2010 RAS survey, total and percentage necromass carbon stock losses in the 18 plots surveyed between 2014 and 2017, and the proportion / area of plots burned during the 2015-16 El Niño, across forest classes of prior human disturbance (Table 1). Linear regression was used to investigate the relationship between: necromass carbon stocks before and after the 2015-16 El Niño; fire intensity and stock losses; and the burned area in each plot and stock losses.

2.4 Quantification of region-wide areal extent of 2015-16 wildfires in central-eastern Amazonia

2.4.1 Overview of approach

A time-series (2010–2016) of Landsat (5, 7, and 8) imagery was classified using a pixel-by-pixel unsupervised *k*-means classification approach. Following visual assessment of the classification and manual correction, the total area of primary and secondary forest burned during the 2015–16 El Niño was calculated.

2.4.2 Input data

A time-series (2010–2016) of Landsat 5, 7, and 8 raw imagery and indices (Appendix 1) was downloaded from the EROS Science Processing Architecture (ESPA)/U.S. Geological Survey (USGS) website (https://espa.cr.usgs.gov). Spectral bands including the visible to medium infrared were used in combination with: the Normalised Difference Vegetation Index (NDVI); Soil adjusted Vegetation Index (SAVI); Enhanced Vegetation Index (EVI), and Normalised Burn Ratio 2 (NBR2; USGS 2016; Table 2). Imagery from Landsat 7 and 8 were used in combination with the panchromatic band to improve the spatial resolution.

2.4.3 Classification

Pixel-by-pixel unsupervised *k*-means classifications (Drake & Hamerly, 2012; MacQueen et al., 1967) of each Landsat image was performed with 10 iterations in ERDAS IMAGE v.16 (Hexagon Geospatial, 2016) to classify primary forest (undisturbed and disturbed), secondary forest, burned forest (from the 2015–2016 El Niño-mediated wildfires), deforested areas, water bodies, and *other* (e.g. agricultural lands and urban structures).

2.4.4 Correction of classifier errors

The classification produced by the unsupervised *k*-means algorithm were then imported and vectorised in ArcGIS v.10.2 (ESRI, 2014). A visual assessment of the classifier accuracy was carried out and any errors were manually corrected in ArcGIS v.10.2 (ESRI, 2014). The vectorised classification was manually compared to each Landsat band and combinations thereof displayed in RGB composites to identify misclassification. Any misclassifications were then corrected manually.

2.5 Estimation of region-wide immediate CO₂ emissions

First, the following equation was developed to estimate the loss of carbon per hectare (*NL*) from the combustion of necromass:

(Eq. 6) $$NL = FL_{CWD} \times (CC_{CWD} - D_{CWD}) + FL_{LLFWD} \times BA$$

where FL_{CWD} is the per ha fuel load of CWD; CC_{CWD} is the combustion completeness of CWD; D_{CWD} is the background decomposition rate measured in unburned control sites; FL_{LLCWD} is the fuel load of leaf litter and FWD per ha; and, BA is the proportion of the plot that burned.

Second, given the current limitations of methods to detect necromass stocks and their spatial distribution in closed canopy tropical forests and the limited number of on-the-ground measures of combustion characteristics, four scenarios were constructed—two for primary forest and two for secondary forests (Table 2). Primary and secondary forests were treated separately because they had significantly different fuel loads and combustion characteristics and were able to be mapped separately. The first primary forest scenario (Prim1) used all data from all primary classes (disturbed and undisturbed) and is the least conservative in that it includes the marginally higher fuel loads found in undisturbed primary forests. This scenario seems the most appropriate at first glance as the wildfires in this region affected both undisturbed and disturbed areas of forest in this region. However, there is evidence to suggest that disturbed primary classes are more vulnerable to combustion (Alencar et al., 2011; Cochrane et al., 1999; Cochrane & Schulze, 1999). The second primary forest scenario (Prim2) is the more conservative scenario of the two as it only includes the lower fuel loads found in the disturbed classes of primary forest. The first secondary forest scenario (Sec1)

is the least conservative of the two secondary forest scenarios as, in an effort to increase decomposition rate and burned area sample sizes, data from all primary forest classes were included. The second secondary forest scenario (Sec2) was more conservative, including only data from secondary forests on decomposition rates and burned area. Due to the lack of data on combustion completeness of CWD (CC_{CWD}) in secondary forests, both secondary forest scenarios (Sec1 and Sec2) used CC_{CWD} values from primary forests. Finally, to determine the means and standard errors of the variables used in Eq. 6 for each scenario described above 1000 bootstrap with replacement simulations were run. The standard error of Eq. 6 was calculated using the variable standard errors, accounting for error propagation, and 95% confidence intervals for Eq. 6 were constructed as its mean value ± 1.96 times the standard error of the mean.

Table 2. Forest classes included in each of the four (two for primary forest and two for secondary forest) land-use scenarios and their associated sample sizes. FL_{CWD} = Coarse Woody Debris (CWD) Fuel Load; CC_{CWD} = CWD Combustion Completeness; D_{CWD} = CWD Decomposition rate; FL_{LLFWD} = Fuel Load of leaf litter and Fine Woody Debris combined; and BA = Burned Area. Prim1 is the least conservative primary forest scenario, including data from all primary classes, including undisturbed primary forest that contained high necromass stocks. Prim2 is more conservative, using only data from the disturbed classes that had lower necromass stocks. Sec1, the least conservative of the two secondary forest scenarios, using data D_{CWD} and BA data from primary forests to increase sample sizes. Sec2 was the most conservative secondary forest scenario using data only from secondary forest, except for CC_{CWD} data from primary forest which was used by both secondary forest scenarios (Sec1 and Sec2) due to a lack of data in secondary forests.

Scenario	FL_{CWD}	CC_{CWD}	D_{CWD}	FL_{LLFWD}	BA
Prim1	All primary classes ($n = 74$)	All primary classes ($n = 7$)	All primary classes ($n = 7$)	All primary classes ($n = 74$)	All primary classes ($n = 15$)
Prim2	Disturbed primary classes only ($n = 57$)	Disturbed primary classes only ($n = 5$)	Disturbed primary classes only ($n = 4$)	Disturbed primary classes only ($n = 47$)	Disturbed primary classes only ($n = 10$)
Sec1	Secondary forests only ($n = 39$)	All primary classes ($n = 7$)	All classes ($n = 10$)	Secondary forests only only ($n = 39$)	All classes ($n = 17$)
Sec2	Secondary forests only ($n = 39$)	All primary classes ($n = 7$)	Secondary forests only ($n = 3$)	Secondary forests only ($n = 39$	Secondary forests only ($n = 2$)

2.6 Comparison with GFED4.1s and GFAS 1.1

The region-wide CO_2 emission estimates were compared with two fire emissions databases frequently used in earth systems models and carbon budgets: the Global Fire Emissions Database (GFED) version 4.1s (van der Werf et al., 2017) and the Global Fire Assimilation System (GFAS) version 1.1 (Kaiser et al., 2012). Both datasets, were obtained for the study period (August 2015–July 2016) and cropped to the approximately 6.5 Mha study region, shown in Figure 1.

The CO_2 emissions estimated here were plotted spatially along with those of GFED and GFAS—at 0.25° and 0.1°, respectively—to investigate potential sources of discrepancy between the estimates. To map the CO_2 emissions estimated in the present study it was assumed that the emissions in each pixel were proportional to area burn (i.e. assuming the density of carbon and combustion and decompositions characteristics were spatially invariable).Finally, because GFED also provides estimates of the area burned at 0.25°, the burned area map produced for this study was used to estimate burned area at the same resolution so they could be compared.

3 RESULTS I: PLOT-LEVEL ESTIMATES OF FUEL COMBUSTION AND BURN PATTERNS

3.1 Necromass stocks across humid tropical forests

Total necromass and its components measured in 2010 during the RAS survey (Berenguer et al., 2014; Gardner et al., 2013), varied significantly by forest class (p < 0.05 in all cases; Figure 1). Primary forests contained significantly higher total necromass than secondary forests (p < 0.01 for all pairwise comparisons), with the highest total found in undisturbed primary forests (30.2 ± 2.1 Mg ha^{-1}, mean ± se). In contrast, secondary forests contained only half as much necromass as undisturbed primary forests (15.6 ± 3.0 Mg ha^{-1}). Variation in total necromass was driven in large part by variation in CWD, which accounted for 61.3 ± 2.7% of the total necromass stocks across forest classes. Leaf litter was the next most important component of total necromass, with 19.8 ± 2.7% residing in this component. Dead standing stems accounted for 14.4 ± 1.8% of total necromass. Finally, FWD was by far the smallest necromass component, comprising just 4.6 ± 0.2% of the total.
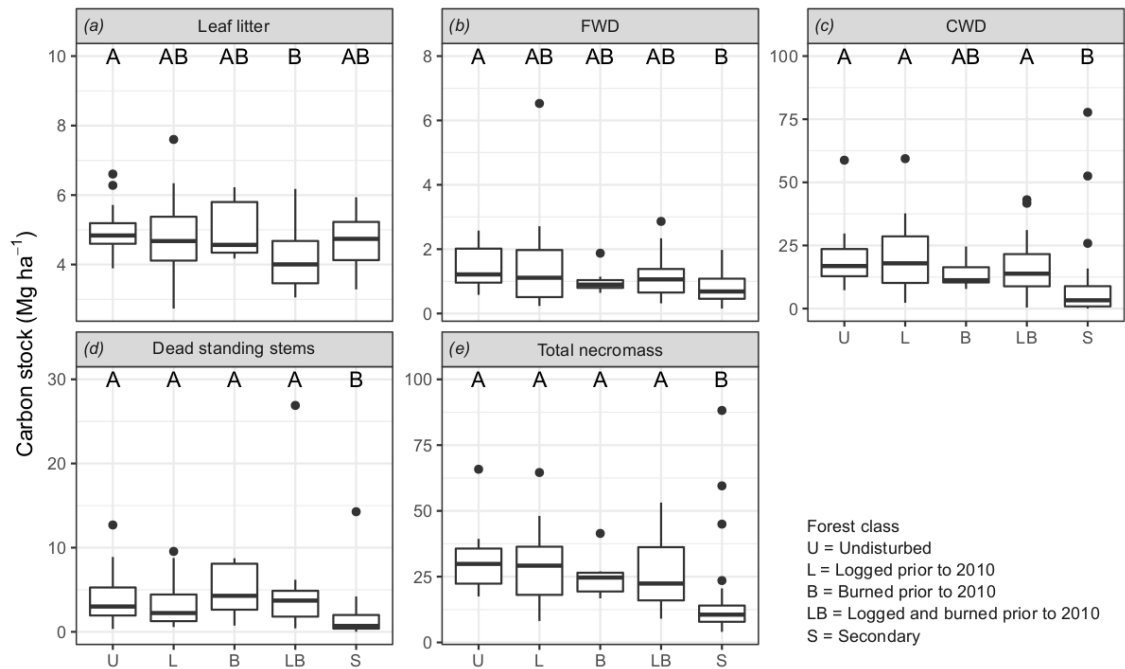
Figure 1. Necromass carbon stocks in leaf litter (a), fine woody debris (FWD; b), coarse woody debris (CWD; c), dead-standing stems (d), and the total across all components (e) in human-modified Amazonian forests. Boxes show the interquartile range and dots show outliers. Letters above the boxplots show the results from multiple pairwise comparisons of forest class medians. Classes that do not share a letter have significantly different medians ($p < 0.05$).

3.2 Impact of El Niño-mediated wildfires on necromass stocks

On average, 87.1 ± 2.7% of the ground area of the fire-affected study plots burned, and there was no significant difference in the total burned area of fire-affected plots across forest classes (χ^2_3 = 2.1; p = 0.56). From the 88 CWD pieces measured before the fires, 54 completely burned, 32 partially burned, and two were untouched by fire. CWD carbon stocks losses from combustion varied from 38% to 94% (mean = 65.4%, SE = 7.1%) at the plot-level.

Necromass carbon stock losses in the seven burned plots were unrelated to median char height ($R^2 = 0.09$; $p = 0.51$; Figure 2a) and area of plot burned ($R^2 = 0.10$; $p = 0.49$; Figure 2b). Forest class did not predict necromass carbon stock losses in burned sites when expressed as either percentage ($\chi^2_2 = 2.25$; $p = 0.32$) or total ($\chi^2_2 = 1.12$; $p = 0.57$) loss. Similarly, forest class did not predict necromass losses in unburned sites when expressed as either percentage ($\chi^2_3 = 1.58$; $p = 0.66$) or total ($\chi^2_3 = 2.18$; $p = 0.54$) loss.
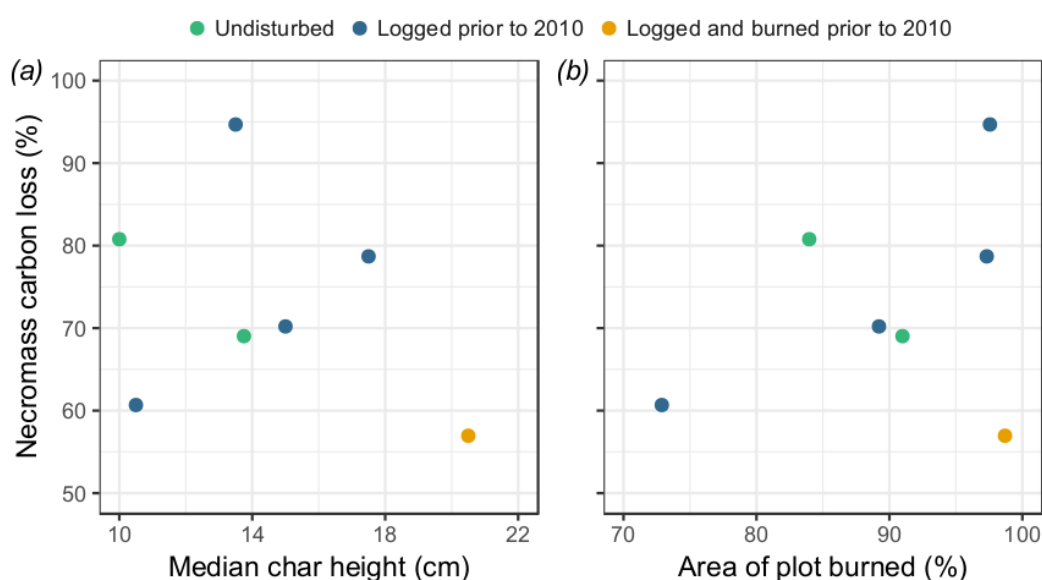
Figure 2. (*a*) Necromass carbon stock losses and fire intensity, as measured by median char height. (*b*) Necromass carbon stock losses and area of plot burned.

On average, burned sites lost 73.0 ± 4.9% of their pre-El Niño necromass stocks (Figure 3), compared to a 26.1 ± 4.8% reduction in unburned sites (from decomposition). As expected, pre-El Niño necromass stocks strongly predicted post-El Niño necromass in unburned sites ($R^2 = 0.95$; $p < 0.001$; Figure 3a). This relationship disappeared in fire-affected plots ($R^2 = 0.08$; $p = 0.54$; Figure 3b), indicating that combustion completeness was insensitive to initial necromass stocks. Despite the small sample sizes, visual inspection suggests that these findings were unaffected by forest class.
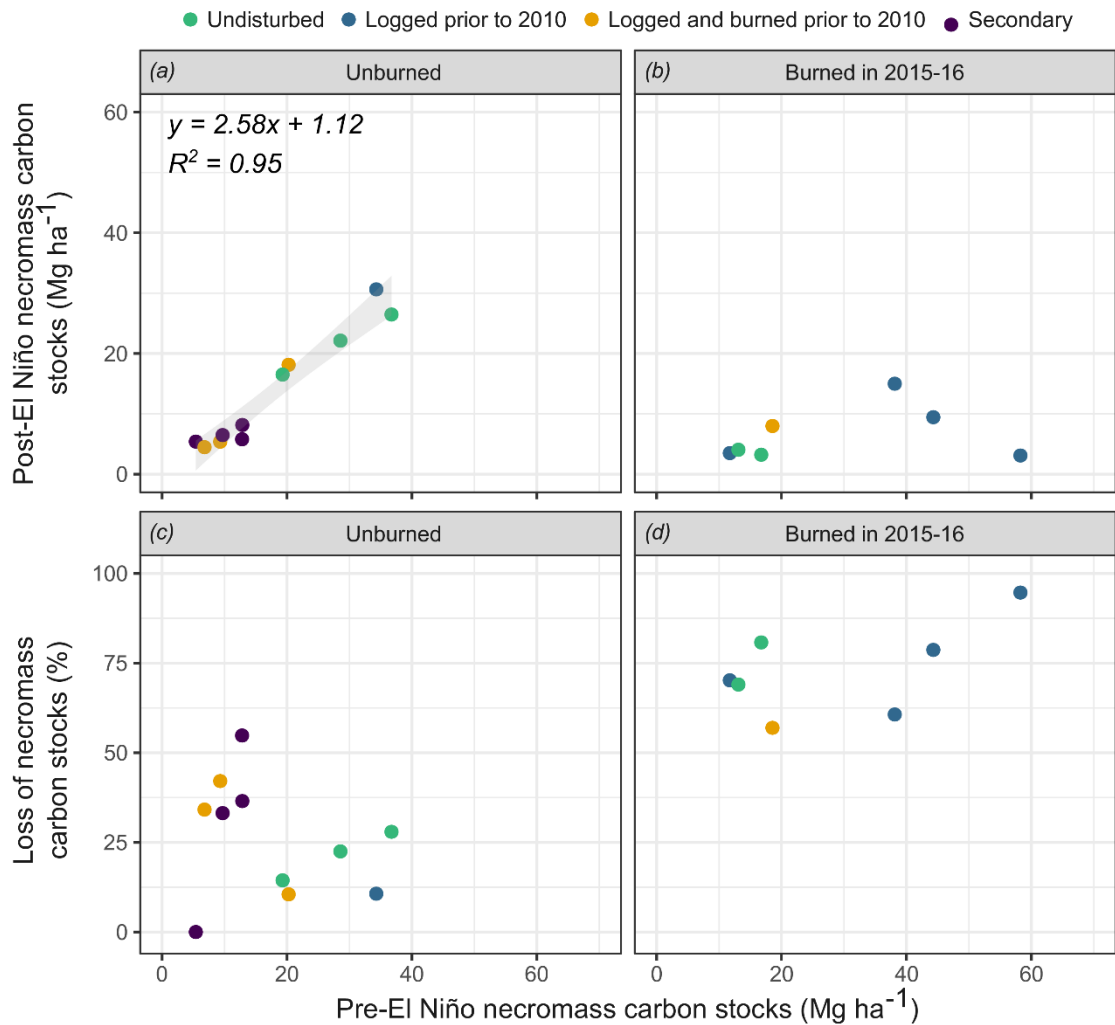
Figure 3. Pre- vs post-El Niño necromass carbon stocks in unburned sites (a) and sites burned during 2015-16 (b), and pre-El Niño necromass carbon stocks vs post-El Niño necromass carbon stock losses in unburned sites (c) and sites burned during 2015-16 (d) in human-modified Amazonian forests. In panel (a) the black line shows the significant ($p < 0.001$) relationship between pre- and post-El Niño necromass carbon stocks in unburned sites. The equation for this relationship is shown in the panel. The grey band represents 1 s.e.m. Note that, due to data limitations, pre- and post-El Niño necromass totals are based on coarse and fine woody debris and leaf litter only (i.e. standing-dead stems are not included. These, however, account for a small (~10–15 %) proportion of necromass stocks (Figure 1)).

4 RESULTS II: REGION-WIDE BURNED AREA

During the 2015-16 El Niño, 982,276 ha (15.2%) of forest in the study region experienced understorey wildfires, which were spread over two states, three protected areas, and 14 municipalities. Wildfires were overwhelmingly concentrated in primary (including disturbed and undisturbed) forests: <2% occurred in secondary forests, despite these accounting for 9% of the forest cover in our study region.
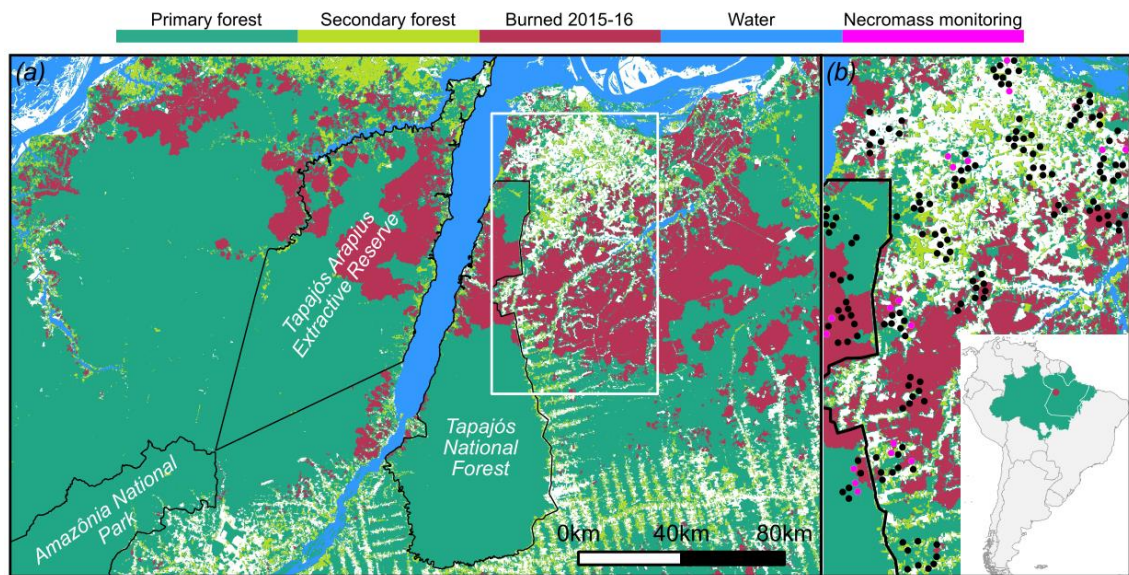
Figure 4. (a) Map of the area burned during the 2015-16 fires and the 2017 land-uses across the ~6.5 million ha study region. (b) The land-use map within the RAS study area (shown by the white border in (a)). Also shown in this panel are the locations of the 107 study plots (black circles). The 18 of these that were used for necromass monitoring are shown as orange circles. The inset shows the Santarém study region (red circle) within South America, the Brazilian Amazon (green), and Pará (white border).

5 RESULTS III: REGION-WIDE CO_2 EMISSIONS AND COMPARISON WITH GFED4.1S AND GFAS

In Scenario **a** (Figure 5), which considers all primary and secondary forests (Prim1 + Sec1; Table 2), necromass carbon stock losses amounted to 10.06 Tg (95% confidence interval, 5.85-14.27 Tg). Converting to CO_2, this is equivalent to expected emissions of 33.05 Tg (95% confidence interval, 19.22-46.87 Tg; Figure 5). Mean CO_2 emission estimates were relatively insensitive to the land-use scenarios (Section 2.5; Table 2; Figure 5). However, the 95% confidence interval was substantially wider with land-use scenario prim2 (scenarios **b** & **d**; Figure 5) as the sample size of decomposition rates was substantially smaller when restricted to disturbed primary forest only compared with all primary forests (prim1)—undisturbed and disturbed—combined.
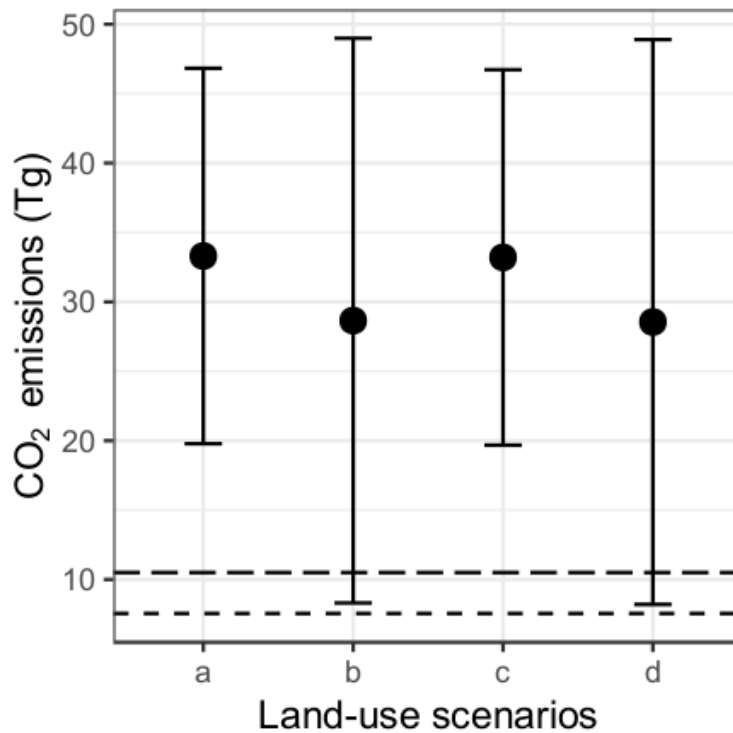
Figure 5. Immediate CO_2 emissions for wildfires in central-eastern Amazonian human-modified tropical forests. Points show expected emissions for four land-use scenarios (see Section 2.5; Table 2): a, Prim1 + Sec1; b, Prim2 + Sec1; c, Prim1 + Sec2; d, Prim2 + Sec2. Error bars show 95% confidence intervals. Also shown are cumulative CO_2 emissions for our study region and period from the Global Fire Emissions Database (GFED4.1s; short-dashed line) and the Global Fire Assimilation System v. 1.1 (GFAS; long-dashed line).

GFED4.1s and GFAS 1.1 both vastly underestimated expected wildfire CO_2 emissions for the study region and period. These databases suggest cumulative emissions that are 77% and 68%, respectively, lower than the expected value found with land-use scenario **a** (Prim1 + Sec1; Figure 5). Highlighting the insensitivity of GFED to understorey wildfires, this database suggested that, 6% of any given 0.25° cell across our study region, and approximately 90, 000 ha in total, burned during the 2015–2016 El Niño (Figure 6*e*). By contrast, the present study shows that as much as 74% of a cell (Figure 6*f*) and almost 1 million ha of forest was affected by understorey wildfires.
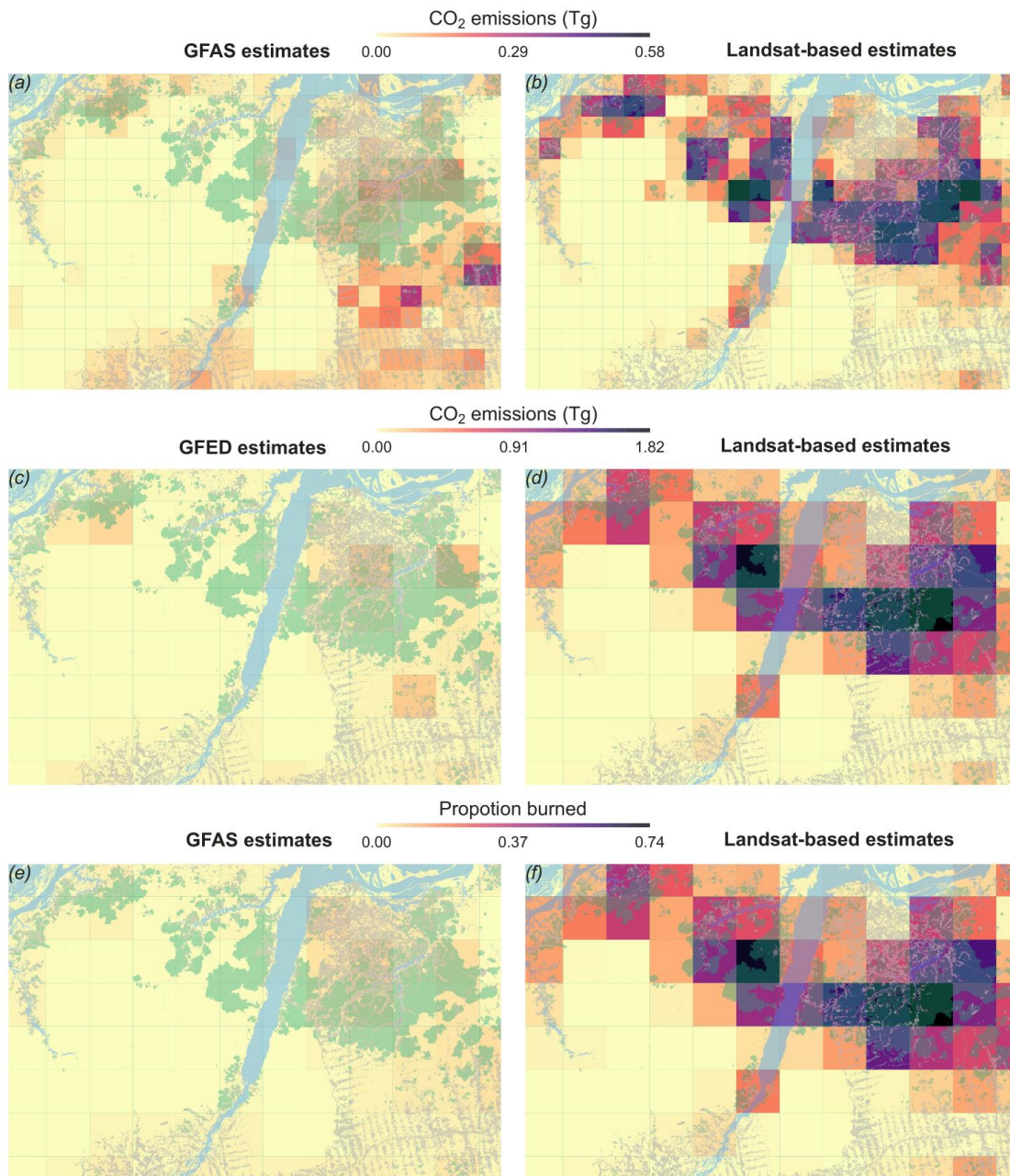
Figure 6. Comparison with the Global Fire Assimilation System (GFAS) and the Global Fire Emissions Database (GFED). Landsat-based CO_2 emissions for the region and period of the present study from GFAS (a) and the emissions estimated here shown at the same scale (0.1 degrees; (b)). CO_2 emissions from GFED (c) and the emissions estimated here shown at the same scale (0.25 degrees; (d)). The proportion of land burned for the study region and period of the present study from GFED (e) and the burned area estimated here shown at the same scale (0.25 degrees; (f)). In all panels, the Landsat-derived fire map in the present study is shown in dark green, deforestation in light grey, and water in blue.

6 DISCUSSION, GENERAL CONCLUSIONS, AND RECOMMENDATIONS

6.1 Interpretation of results

Mean total necromass (standing-dead stems, CWD, FWD, and leaf litter) carbon stocks in undisturbed forests (30.2 ± 2.1 Mg ha^{-1}) found here were broadly consistent with previous estimates for the eastern Amazon. For example, Keller et al. (2004) and Palace et al. (2007) found necromass of, respectively, 25.4 and 29.2 Mg ha^{-1} in undisturbed primary forests in the Tapajós region of Pará. However, in primary forests disturbed by reduced-impact logging, these studies found, respectively, 36.4 and 42.7 Mg ha^{-1} of necromass carbon, while the estimates found here for necromass stocks in disturbed primary forests are markedly lower (Figure 1*e*). This discrepancy is likely a function of time since disturbance, as Keller et al. (2004) and Palace et al. (2007) assessed necromass carbon stocks soon after disturbance, when necromass stocks were likely to be higher. In contrast, disturbance of RAS sites occurred between 1.5 and 25 years before the 2010 surveys. Necromass stocks can be highly dynamic, with residence times for most coarse woody debris estimated at less than a decade (Palace et al., 2012),

especially in the case of small diameter and low wood density tree species (Chambers et al., 2000). Thus, necromass stocks in many of the disturbed primary forest sites studied here may have had time to decrease to an equilibrium level, similar to that of undisturbed forests, where input and decomposition are largely balanced

There were, however, significantly larger necromass stocks in primary forests compared to secondary forests. This may be explained by a) pre-abandonment land-uses removing all fallen biomass in intensive clearance or maintenance fires; b) the smaller necromass input pool in secondary forests due to lower aboveground live biomass (Berenguer et al., 2014); and c) the lower wood density of stems in secondary forests (Berenguer et al., 2018), resulting in more rapid coarse woody debris decomposition.

On average, wildfires burned 87.1 ± 2.7% of the fire-affected necromass monitoring plots (Figure 3b). This figure is substantially higher than the 62-75% burn coverage measured during experimental fires in previously undisturbed transitional Amazonian forests (Brando et al., 2016). The areal extent of these wildfires reduced necromass (in CWD, FWD, and leaf litter) carbon stocks by 46.9 ± 6.9%, when gross necromass loss (73.0 ± 4.9%) was corrected for decomposition (26.1 ± 4.8%).

The areal extent of these wildfires at the plot-level was not explained by forest disturbance class. This may indicate that the 2015-16 El Niño, which was one of strongest on record, with particularly strong drought conditions in eastern Amazonia (Jiménez-Muñoz et al., 2016), reduced necromass moisture content across all forest classes to a level which permitted combustions and sustained wildfires, overriding any pre-existing microclimatic differences that may have existed due to the initial disturbance. This is further corroborated by the fact that wildfires did not distinguish between largely undisturbed forests (mostly inside protected areas) and those that have been modified by humans (mostly outside protected areas), burning vast areas of both types of forest (Figure 4).

Interestingly, the areal extent of the wildfires at the plot-level also did not explain the percentage loss of necromass stocks. Perhaps this was simply due to the small sample sizes used, or maybe this was a result of sporadic fuel loads (especially CWD).

The understorey wildfires that affected the burned plots were relatively low intensity, with maximum median char height of 20.5 cm. Median char-height, taken as a proxy of fire intensity, at the plot level did not explain necromass stock losses. Perhaps this was because even the lowest intensity fires were sufficient to consume a significant proportion of the necromass stocks they came in to contact with. Whatever the causal factors, these findings demonstrate that low-intensity wildfires can dramatically diminish necromass stocks in human-modified tropical forests.

This novel assessment revealed that expected immediate necromass CO_2 emissions from these wildfires are around 30 Tg (Figure 5). Putting the magnitude of this issue into context, the estimated CO_2 emissions for the 2015–16 wildfires in eastern Amazonia, that affected an area of <0.2% of the Brazilian Amazon, were equivalent to those from fossil fuel combustion and the production of cement in Denmark, or 6% of such emissions from Brazil, in 2014 (Bank, 2018). Consequently, wildfire-mediated immediate carbon emissions, which are not currently considered under national greenhouse gas inventories (Bustamante et al., 2016), represent a large source of CO_2 emissions. Moreover, these immediate emissions will be greatly exacerbated by further committed emissions resulting from tree mortality, which can be as high as 50% even from low-intensity understorey wildfires (Barlow et al. 2003) and may not be balanced by post-fire regrowth on decadal time scales (Silva et al., 2018) .

Both GFED and GFAS estimated substantially lower CO_2 emissions for wildfires in this region of the Amazon during the 2015–16 El Niño. These databases suggest cumulative emissions that are 77% and 68% lower than the expected value found with land-use scenario a, respectively (prim1 + sec1; Figure

5). These discrepancies are likely the result of underdetection of understorey wildfires by both GFED and GFAS algorithms. GFED and GFAS use Moderate Resolution Imaging Spectroradiometer (MODIS) products that have a spatial resolution of 500 m to 1 km, while the present study uses Landsat imagery and derived indices, with a spatial resolution of 15–30 m, which are commonly considered reference data for validating global products of burned area (Hantson et al., 2013) and Landsat data were indeed used to validate the MCD64A1 MODIS data product used by GFED (Giglio et al., 2018). The underdetection of burned area by GFED and GFAS can be seen across the whole study region but is particularly evident in areas free from historic deforestation (Figure 6). GFED and GFAS appeared to be more successful at detecting fires in agricultural areas (Figure 6)—which have lower fuel loads and were excluded from the present study—perhaps due to the lower levels of forest cover (Figure 6).

6.2 Wider implications of results

On balance, it is likely that the necromass stock loss and carbon emission estimates presented here are highly conservative. First, wildfire-induced carbon changes in the soil organic layer were not measured, yet research from the same region suggests that wildfires significantly reduce soil carbon pools (Durigan et al., 2017); nor was combustion of dead-standing stems estimated, which accounted for ~15% of total necromass (Figure 1). Second, none of the disturbed primary forest plots in which necromass changes were monitored were recently disturbed prior to the 2015-16 wildfires, allowing time for decomposition to reduce high levels of post-disturbance necromass. Had the dataset included recently disturbed sites, necromass losses would likely have been greater. Third, detection of low intensity understorey wildfires continues to present a remote sensing challenge. Although manual correction of our unsupervised land-use classifications revealed only a small number of misclassifications (commissions), it is quite possible that some wildfire-affected sites were missed, leading to an underestimation of regional emissions.

In addition to showing that wildfire carbon emissions can be substantial, the present study has also shown that such emissions remain poorly quantified. GFED and GFAS, CO_2 emission databases that are widely used in Earth Systems models and carbon budgets, returned considerably lower emission estimates for this study region and period than found here (Figure 5). If this pattern of underestimation holds true for the rest of the humid tropics, where dense canopies are present, then global estimates of fire-induced CO_2 emissions may be vastly underestimated. Nevertheless, the scale of the discrepancy between the CO_2 emitted during these wildfires and the estimates of GFED and GFAS may well be underestimated for several reasons. First, this study focused solely on necromass carbon losses from understory wildfires in extant forests whereas GFED and GFAS include emissions from all land use classes combined (Kaiser et al., 2012; van der Werf et al., 2017). Both databases therefore account for grassland and agricultural fires, which can affect large areas of human-modified tropical landscapes. Second, GFED includes both committed and immediate CO_2 emissions (van der Werf et al., 2017). Third, and again with respect to GFED, fuel loads are much high than those present in the post-disturbance plots studied here, because they are primarily derived from slash-and-burn and deforestation studies (van der Werf et al., 2017). Thus, if the degree of underestimation in terms of burned area and CO_2 emissions is similar across the whole Amazon, not only will the CO_2 emissions from low-intensity understorey wildfires be substantially underestimated and the earth system models which rely on them have biased inputs, but broader ecological and social issues will also be underestimated.

The present study adds to work on prescribed burns associated with deforestation (van Leeuwen et al., 2014), contributing important information about the role of El Niño-mediated wildfires. The scale of the immediate emissions we estimated, coupled with future committed emissions, make wildfires particularly relevant to climate change mitigation programmes such as REDD+ (Aragão and Shimabukuro 2010; Barlow et al. 2012). The results presented here show that legally protected areas in the Amazon rainforest can be substantially affected by uncontrolled understorey wildfires during extreme drought conditions. Thus, for REDD+ to succeed in Amazonia, forests must be protected from wildfires,

as agricultural fires quickly become uncontrollable and spread to protected areas which have historically served as carbon stores (Soares-Filho et al., 2010), as illustrated by the large areas burned in the Tapajós National Forest and the Tapajós-Arapiuns Extractive Reserve (Figure 4). Thus, undermining the role of and investments in protected areas for climate change mitigation programmes. Even the immediate emissions from large-scale wildfires can equal those from whole countries. Moreover, the committed emissions from such fires are expected to be many times greater due to delayed tree mortality and arrested regrowth/carbon sequestration in affected forests (Silva et al., 2018). Future climate change will make this only more imperative, with extreme droughts, higher temperatures, and reduced rainfall all predicted for the Amazon basin in the near future (Dai, 2013; Spracklen & Garcia-Carreras, 2015).

6.3 Future research

6.3.1 Larger datasets

Although the pre- and post-fire dataset presented here is the first of its kind, which allows for the quantification of necromass carbon stocks following uncontrolled understorey wildfires in human-modified Amazonian forests, the sample sizes were limited, with just 18 necromass monitoring plots, of which seven burned during the 2015-16 El Niño. Consequently, these results should be treated with a degree of caution. In particular, necromass stock losses were not significantly related to the plot-level estimates of burned area, and fire susceptibility did not appear to vary across disturbance classes. In both cases, the lack of significance may reflect the small sample sizes rather than a genuine lack of relationship. Moreover, due to the small sample sizes used to construct the region-wide CO_2 immediate emissions scenarios, the 95% confidence intervals are wide—ranging from around 8 Tg to almost 48 Tg (Figure 5). Therefore, to better constraint these values future research efforts should prioritise necromass monitoring in larger plots and numbers of sites, across a range of tropical forests

and land-use scenarios, incorporating sites of different ages/times since disturbance, canopy thickness, and landscape contexts.

6.3.2 Reduced susceptibility of secondary forests

The present study has shown that secondary forests exhibit a reduced susceptibility to sustained combustion during wildfires mediated by severe drought events. This may be due to wildfires spreading less easily through secondary forest due to lower (see Figure 1) and more sporadic fuel loads. Another influence may be the lower night-time temperatures experienced in secondary forests owing to lower density canopies, or complete lack thereof. For example, day and night-time temperatures can vary substantially, with open areas experiencing surface soil temperatures as high as 42 °C during the day and as low as 25 °C during night-time (Bazzaz & Pickett, 1980). Though this disparity diminishes as canopy cover returns (Bazzaz & Pickett, 1980), as it is commonly noted that wildfires burn less intensely even in primary forests during night-time (De Faria et al., 2017), this reduction in night-time temperatures may be sufficient, along with lower fuel loads, to stifle wildfires in secondary forests. Elucidating these causal factors will help to improve global fire models and constrain further emissions estimates by allowing spatial mapping of emissions and combustion characteristics.

6.3.3 Improved detection and mapping of wildfires

The present study has shown that GFED4.1s and GFAS both significantly underestimated the impact of the 2015-16 El Niño-mediated wildfires of the central-eastern Amazon. GFED4.1s underestimated burned area in the central-eastern Amazon by a factor of 10 during the wildfires experienced during the 2015-16 El Niño-mediated drought. GFED uses the Moderate Resolution Imaging Spectroradiometer (MODIS) product MCD64A1 (collection 5.1), which spatially maps burned area at a resolution of 500m—much greater than the 30m spatial

resolution used in the present study. Earlier versions of the algorithm were criticized for underestimating burned area (van der Werf et al., 2017). In an effort to reduce this bias, the algorithms of Randerson et al., (2012) for detecting *small* fires using the MODIS 1-km thermal anomalies (*active fires*) product MOD14A1 were extended and incorporated into the GFED algorithm (van der Werf et al., 2017). The incorporation of *small* fires has significantly boosted the detection of burned area globally (van der Werf et al., 2017). Yet in the case of humid tropical forests, which generally have dense closed canopies and experience relatively low-intensity understorey wildfires, burned area is evidently still substantially underestimated. GFAS uses empirical relationships between fire radiative power (FRP), as measured by the MODIS Aqua and Terra satellites, and dry matter combustion rates and gas species emissions rates without estimating burned area (Kaiser et al., 2012). This approach is much less demanding computationally and for this particular study region and period, has been more successful at capturing the CO_2 emissions from the understorey wildfires in central-eastern Amazonia. However, this approach does not estimate burned area (Kaiser et al., 2012), which is essential for estimating committed emission and other ecosystem-level impacts because biomass stocks (Marvin et al., 2014; Saatchi et al., 2007) and other ecosystem properties (Fyllas et al., 2009; Quesada et al., 2012) vary spatial across the Amazon. Future research should prioritise the development of burn area products using higher resolution imagery, or active remote sensing systems such as synthetic-aperture radar (SAR) (see Lohberger et al., 2018 for recent example) to better quantify the extent and impacts of understorey wildfires in humid tropical forests.

7 CONCLUSION

The present study has demonstrated that there was a substantial loss of necromass following El Niño-mediated wildfires in the central-eastern Amazon during 2015-16. These wildfires burned 982,276 ha (15.2% of the study region) of primary and secondary forest, resulting in expected immediate CO_2 emissions of approximately 30 Tg. A better understanding of this large and poorly quantified source of atmospheric carbon is crucial for climate change mitigation efforts, and will only become more imperative as extreme droughts, higher temperatures, and reduced rainfall create conditions even more conducive to wildfires across the Amazon basin in the near future.

8 REFERENCES

Alencar, A., Asner, G. P., Knapp, D., & Zarin, D. (2011). Temporal variability of forest fires in eastern Amazonia. *Ecological Applications*, *21*(7), 2397–2412. https://doi.org/10.1890/10-1168.1

Alencar, A., Nepstad, D., Diaz, M. C. V., Alencar, A., Nepstad, D., & Diaz, M. C. V. (2006). Forest Understory Fire in the Brazilian Amazon in ENSO and Non-ENSO Years: Area Burned and Committed Carbon Emissions. *Earth Interactions*, *10*(6), 1–17. https://doi.org/10.1175/EI150.1

Aragão, L. E. O. C., Anderson, L. O., Fonseca, M. G., Rosan, T. M., Vedovato, L. B., Wagner, F. H., … Saatchi, S. (2018). 21st Century drought-related fires counteract the decline of Amazon deforestation carbon emissions. *Nature Communications*, *9*(1), 536. https://doi.org/10.1038/s41467-017-02771-y

Aragão, L. E. O. C., & Shimabukuro, Y. E. (2010). The incidence of fire in Amazonian forests with implications for REDD. *Science*, *328*(5983), 1275–1278. https://doi.org/10.1126/science.1186925

Baccini, A., Walker, W., Carvalho, L., Farina, M., Sulla-Menashe, D., & Houghton, R. A. (2017). Tropical forests are a net carbon source based on aboveground measurements of gain and loss. *Science (New York, N.Y.)*, *358*(6360), 230–234. https://doi.org/10.1126/science.aam5962

Ballantyne, A. P., Alden, C. B., Miller, J. B., Tans, P. P., & White, J. W. C. (2012). Increase in observed net carbon dioxide uptake by land and oceans during the

past 50 years. *Nature*, *488*(7409), 70–72. https://doi.org/10.1038/nature11299

Bank, W. (2018). CO2 emissions. Retrieved April 27, 2018, from https://data.worldbank.org/indicator/EN.ATM.CO2E.KT?view=chart

Barlow, J., Lennox, G. D., Ferreira, J., Berenguer, E., Lees, A. C., Nally, R. Mac, … Gardner, T. A. (2016). Anthropogenic disturbance in tropical forests can double biodiversity loss from deforestation. *Nature*, *535*(7610), 144–147. https://doi.org/10.1038/nature18326

Barlow, J. M., Palmer, P. I., Bruhwiler, L. M., & Tans, P. (2015). Analysis of CO2mole fraction data: First evidence of large-scale changes in CO2uptake at high northern latitudes. *Atmospheric Chemistry and Physics*, *15*(23), 13739–13758. https://doi.org/10.5194/acp-15-13739-2015

Barlow, J., Parry, L., Gardner, T. A., Ferreira, J., Aragão, L. E. O. C., Carmenta, R., … Cochrane, M. A. (2012). The critical importance of considering fire in REDD+ programs. *Biological Conservation*, *154*, 1–8. https://doi.org/10.1016/j.biocon.2012.03.034

Barlow, J., & Peres, C. A. (2004). Ecological responses to El Nino-induced surface fires in central Brazilian Amazonia: management implications for flammable tropical forests. *Philosophical Transactions of the Royal Society B: Biological Sciences*, *359*(1443), 367–380. https://doi.org/10.1098/rstb.2003.1423

Barlow, J., Peres, C. A., Lagan, B. O., & Haugaasen, T. (2003). Large tree mortality and the decline of forest biomass following Amazonian wildfires. *Ecology Letters*, *6*(1), 6–8. https://doi.org/10.1046/j.1461-0248.2003.00394.x

Bazzaz, F. A., & Pickett, S. T. A. (1980). *PHYSIOLOGICAL ECOLOGY OF TROPICAL SUCCESSION: A Comparative Review*. *Ann. Rev. Ecol. SySL* (Vol. 11). Retrieved from www.annualreviews.org

Berenguer, E., Ferreira, J., Gardner, T. A., Aragão, L. E. O. C., De Camargo, P. B., Cerri, C. E., … Barlow, J. (2014). A large-scale field assessment of carbon stocks in human-modified tropical forests. *Global Change Biology*, *20*(12), 3713–3726. https://doi.org/10.1111/gcb.12627

Berenguer, E., Gardner, T. A., Ferreira, J., Aragão, L. E. O. C., Mac Nally, R., Thomson,

J. R., ... Barlow, J. (2018). Seeing the woods through the saplings: Using wood density to assess the recovery of human-modified Amazonian forests. *Journal of Ecology*, 0–2. https://doi.org/10.1111/1365-2745.12991

Boers, N., Marwan, N., Barbosa, H. M. J., & Kurths, J. (2017). A deforestation-induced tipping point for the South American monsoon system. *Scientific Reports*, *7*(1), 41489. https://doi.org/10.1038/srep41489

Brando, P. M., Oliveria-Santos, C., Rocha, W., Cury, R., & Coe, M. T. (2016). Effects of experimental fuel additions on fire intensity and severity: unexpected carbon resilience of a neotropical forest. *Global Change Biology*, *22*(7), 2516–2525. https://doi.org/10.1111/gcb.13172

Brienen, R. J. W., Phillips, O. L., Feldpausch, T. R., Gloor, E., Baker, T. R., Lloyd, J., ... Zagt, R. J. (2015). Long-term decline of the Amazon carbon sink. *Nature*, *519*(7543), 344–348. https://doi.org/10.1038/nature14283

Bush, M. B., Silman, M. R., de Toledo, M. B., Listopad, C., Gosling, W. D., Williams, C., ... Krisel, C. (2007). Holocene fire and occupation in Amazonia: records from two lake districts. *Philosophical Transactions of the Royal Society B: Biological Sciences*, *362*(1478), 209–218. https://doi.org/10.1098/rstb.2006.1980

Bustamante, M. M. C., Roitman, I., Aide, T. M., Alencar, A., Anderson, L. O., Aragão, L., ... Vieira, I. C. G. (2016). Toward an integrated monitoring framework to assess the effects of tropical forest degradation and recovery on carbon stocks and biodiversity. *Global Change Biology*, *22*(1), 92–109. https://doi.org/10.1111/gcb.13087

Cai, W., Borlace, S., Lengaigne, M., van Rensch, P., Collins, M., Vecchi, G., ... Jin, F.-F. (2014). Increasing frequency of extreme El Niño events due to greenhouse warming. *Nature Climate Change*, *4*(2), 111–116. https://doi.org/10.1038/nclimate2100

Chambers, J. Q., Higuchi, N., Schimel, J. P., Ferreira, L. V., & Melack, J. M. (2000). Decomposition and carbon cycling of dead trees in tropical forests of the central Amazon. *Oecologia*, *122*(3), 380–388. https://doi.org/10.1007/s004420050044

Chao, K.-J. J., Phillips, O. L., Baker, T. R., Peacock, J., Lopez-Gonzalez, G., Vásquez Martínez, R., ... Torres-Lezama, A. (2009). After trees die: Quantities and

determinants of necromass across Amazonia. *Biogeosciences*, *6*(8), 1615–1626. https://doi.org/10.5194/bg-6-1615-2009

Chen, Y., Randerson, J. T., Morton, D. C., DeFries, R. S., Collatz, G. J., Kasibhatla, P. S., … Marlier, M. E. (2011). Forecasting Fire Season Severity in South America Using Sea Surface Temperature Anomalies. *Science*, *334*(6057), 787–791. Retrieved from http://www.sciencemag.org/content/334/6057/787.abstract

Ciais, P., Willem, J., Friedlingstein, P., & Munhoven, G. (2013). Carbon and Other Biogeochemical Cycles. In Intergovernmental Panel on Climate Change (Ed.), *Climate Change 2013 - The Physical Science Basis* (pp. 465–570). Cambridge: Cambridge University Press. https://doi.org/10.1017/CBO9781107415324.015

Cochrane, M. A. (2003). Fire science for rainforests. *Nature*, *421*(6926), 913–919. https://doi.org/10.1038/nature01437

Cochrane, M. A., Alencar, J. T., Schulze, R. A., Souza, T. J., Nepstad, W., Lefebvre, C. A., … Davidson. (1999). Positive Feedbacks in the Fire Dynamic of Closed Canopy Tropical Forests. *Science*, *284*(5421), 1832–1835. https://doi.org/10.1126/science.284.5421.1832

Cochrane, M. A., & Schulze, M. D. (1999). Fire as a Recurrent Event in Tropical Forests of the Eastern Amazon: Effects on Forest Structure, Biomass, and Species Composition. *Biotropica*, *31*(1), 2–16. https://doi.org/10.1111/j.1744-7429.1999.tb00112.x

Costa, M. H., Biajoli, M. C., Sanches, L., Malhado, A. C. M., Hutyra, L. R., da Rocha, H. R., … de Araújo, A. C. (2010). Atmospheric versus vegetation controls of Amazonian tropical rain forest evapotranspiration: Are the wet and seasonally dry rain forests any different? *Journal of Geophysical Research*, *115*(G4), G04021. https://doi.org/10.1029/2009JG001179

Cox, P. M., Pearson, D., Booth, B. B., Friedlingstein, P., Huntingford, C., Jones, C. D., & Luke, C. M. (2013). Sensitivity of tropical carbon to climate change constrained by carbon dioxide variability. *Nature*, *494*(7437), 341–344. https://doi.org/10.1038/nature11882

Crowley, T. J. (2000). Causes of Climate Change Over the Past 1000 Years. *Science*, *289*(5477), 270–277. https://doi.org/10.1126/science.289.5477.270

Cummings, D. L., Boone Kauffman, J., Perry, D. A., & Flint Hughes, R. (2002). Aboveground biomass and structure of rainforests in the southwestern Brazilian Amazon. *Forest Ecology and Management*, *163*(1–3), 293–307. https://doi.org/10.1016/S0378-1127(01)00587-4

Dai, A. (2013). Increasing drought under global warming in observations and models. *Nature Climate Change*, *3*(1), 52–58. https://doi.org/10.1038/nclimate1633

Davidson, E. A., De Araüjo, A. C., Artaxo, P., Balch, J. K., Brown, I. F., Mercedes, M. M., … Wofsy, S. C. (2012, January 19). The Amazon basin in transition. *Nature*. Nature Publishing Group. https://doi.org/10.1038/nature10717

De Faria, B. L., Brando, P. M., Macedo, M. N., Panday, P. K., Soares-Filho, B. S., & Coe, M. T. (2017). Current and future patterns of fire-induced forest degradation in Amazonia. *Environmental Research Letters*, *12*(9), 095005. https://doi.org/10.1088/1748-9326/aa69ce

Drake, J., & Hamerly, G. (2012). Accelerated k-means with adaptive distance bounds. In *5th NIPS workshop on optimization for machine learning* (pp. 42–53).

Durigan, M. R., Cherubin, M. R., Camargo, P. B., Ferreira, J. N., Berenguer, E., Gardner, T. A., … Cerri, C. E. P. (2017). Soil Organic Matter Responses to Anthropogenic Forest Disturbance and Land Use Change in the Eastern Brazilian Amazon. *Sustainability*, *9*(3), 379. https://doi.org/10.3390/su9030379

Eggleston, H. S., Intergovernmental Panel on Climate Change. National Greenhouse Gas Inventories Programme, S. ed., Chikyū Kankyō Senryaku Kenkyū Kikan, L. ed., & Miwa, K. (2006). *2006 IPCC guidelines for national greenhouse gas inventories*. Kanagawa, JP : Institute for Global Environmental Strategies. Retrieved from http://www.sidalc.net/cgi-bin/wxis.exe/?IsisScript=earth.xis&method=post&formato=2&cantidad=1&expresion=mfn=001720

ESRI. (2014). Arcgis 10.2.

Ferreira, J., Pardini, R., Metzger, J. P., Fonseca, C. R., Pompeu, P. S., Sparovek, G., & Louzada, J. (2012). Towards environmentally sustainable agriculture in Brazil:

challenges and opportunities for applied ecological research. *Journal of Applied Ecology*, *49*(3), no-no. https://doi.org/10.1111/j.1365-2664.2012.02145.x

Fyllas, N. M., Patiño, S., Baker, T. R., Bielefeld Nardoto, G., Martinelli, L. A., Quesada, C. A., … Lloyd, J. (2009). Basin-wide variations in foliar properties of Amazonian forest: phylogeny, soils and climate. *Biogeosciences*, *6*(11), 2677–2708. https://doi.org/10.5194/bg-6-2677-2009

Gardner, T. A., Ferreira, J., Barlow, J., Lees, A. C., Parry, L., Vieira, I. C. G., … Zuanon, J. (2013). A social and ecological assessment of tropical land uses at multiple scales: the Sustainable Amazon Network. *Philosophical Transactions of the Royal Society B: Biological Sciences*, *368*(1619), 20120166–20120166. https://doi.org/10.1098/rstb.2012.0166

Gatti, L. V., Gloor, M., Miller, J. B., Doughty, C. E., Malhi, Y., Domingues, L. G., … Lloyd, J. (2014). Drought sensitivity of Amazonian carbon balance revealed by atmospheric measurements. *Nature*, *506*(7486), 76–80. https://doi.org/10.1038/nature12957

Ghazoul, J., & Chazdon, R. (2017). Degradation and Recovery in Changing Forest Landscapes: A Multiscale Conceptual Framework. *Annual Review of Environment and Resources*, *42*(1), 161–188. https://doi.org/10.1146/annurev-environ-102016-060736

Giglio, L., Boschetti, L., Roy, D. P., Humber, M. L., & Justice, C. O. (2018). The Collection 6 MODIS burned area mapping algorithm and product. *Remote Sensing of Environment*, *217*, 72–85. https://doi.org/10.1016/J.RSE.2018.08.005

Goetz, S. J., Hansen, M., Houghton, R. A., Walker, W., Laporte, N., & Busch, J. (2015). Measurement and monitoring needs, capabilities and potential for addressing reduced emissions from deforestation and forest degradation under REDD+. *Environmental Research Letters*, *10*(12), 123001. https://doi.org/10.1088/1748-9326/10/12/123001

Hansen, J., & Sato, M. (2001). Trends of measured climate forcing agents. *… of the National Academy of Sciences*, *98*(26), 14778–14783. https://doi.org/10.1073/pnas.261553698

Hantson, S., Padilla, M., Corti, D., & Chuvieco, E. (2013). Strengths and weaknesses of MODIS hotspots to characterize global fire occurrence. *Remote Sensing of Environment*, *131*, 152–159. https://doi.org/10.1016/J.RSE.2012.12.004

Hexagon Geospatial. (2016). ERDAS Image 16.

Hoorn, C., Wesselingh, F. P., ter Steege, H., Bermudez, M. A., Mora, A., Sevink, J., … Antonelli, A. (2010). Amazonia through time: Andean uplift, climate change, landscape evolution, and biodiversity. *Science (New York, N.Y.)*, *330*(6006), 927–931. https://doi.org/10.1126/science.1194585

Houghton, R. A., Baccini, A., & Walker, W. S. (2018). Where is the residual terrestrial carbon sink? *Global Change Biology*, *24*(8), 3277–3279. https://doi.org/10.1111/gcb.14313

Hughes, R. F., Kauffman, J. B., & Jaramillo, V. J. (1999). BIOMASS, CARBON, AND NUTRIENT DYNAMICS OF SECONDARY FORESTS IN A HUMID TROPICAL REGION OF MÉXICO. *Ecology*, *80*(6), 1892–1907. https://doi.org/10.1890/0012-9658(1999)080[1892:BCANDO]2.0.CO;2

INMET. (2018). BDMEP - Banco de Dados Meteorológicos para Ensino e Pesquisa. Retrieved July 15, 2018, from http://www.inmet.gov.br/portal/index.php?r=bdmep/bdmep

Jiménez-Muñoz, J. C., Mattar, C., Barichivich, J., Santamaría-Artigas, A., Takahashi, K., Malhi, Y., … Schrier, G. van der. (2016). Record-breaking warming and extreme drought in the Amazon rainforest during the course of El Niño 2015–2016. *Scientific Reports*, *6*(1), 33130. https://doi.org/10.1038/srep33130

Jolly, W. M., Cochrane, M. A., Freeborn, P. H., Holden, Z. A., Brown, T. J., Williamson, G. J., & Bowman, D. M. J. S. J. S. (2015). Climate-induced variations in global wildfire danger from 1979 to 2013. *Nature Communications*, *6*(May), 1–11. https://doi.org/10.1038/ncomms8537

Jones, C. D., Collins, M., Cox, P. M., & Spall, S. A. (2001). The Carbon Cycle Response to ENSO: A Coupled Climate–Carbon Cycle Model Study. *Journal of Climate*, *14*(21), 4113–4129. https://doi.org/10.1175/1520-0442(2001)014<4113:TCCRTE>2.0.CO;2

Joos, F., & Spahni, R. (2008). *Rates of change in natural and anthropogenic radiative*

forcing over the past 20,000 years. Retrieved from www.pnas.org/cgi/content/full/

Kaiser, J. W., Heil, A., Andreae, M. O., Benedetti, A., Chubarova, N., Jones, L., … van der Werf, G. R. (2012). Biomass burning emissions estimated with a global fire assimilation system based on observed fire radiative power. *Biogeosciences*, *9*(1), 527–554. https://doi.org/10.5194/bg-9-527-2012

Kauffman, J. B., & Uhl, C. (1990). Interactions of Anthropogenic Activities, Fire, and Rain Forests in the Amazon Basin (pp. 117–134). Springer, Berlin, Heidelberg. https://doi.org/10.1007/978-3-642-75395-4_8

Keenan, R. J., Reams, G. A., Achard, F., de Freitas, J. V., Grainger, A., & Lindquist, E. (2015). Dynamics of global forest area: Results from the FAO Global Forest Resources Assessment 2015. *Forest Ecology and Management*, *352*, 9–20. https://doi.org/10.1016/j.foreco.2015.06.014

Keenan, T. F., Prentice, I. C., Canadell, J. G., Williams, C. A., Wang, H., Raupach, M., & Collatz, G. J. (2016). Recent pause in the growth rate of atmospheric CO2 due to enhanced terrestrial carbon uptake. *Nature Communications*, *7*(7), 13428. https://doi.org/10.1038/ncomms13428

Keller, M., Palace, M., Asner, G. P., Pereira, R., & Silva, J. N. M. J. N. M. (2004). Coarse woody debris in undisturbed and logged forests in the eastern Brazilian Amazon. *Global Change Biology*, *10*(5), 784–795. https://doi.org/10.1111/j.1529-8817.2003.00770.x

Khanna, J., Medvigy, D., Fueglistaler, S., & Walko, R. (2017). Regional dry-season climate changes due to three decades of Amazonian deforestation. *Nature Climate Change*, *7*(3), 200–204. https://doi.org/10.1038/nclimate3226

Kunert, N., Aparecido, L. M. T., Wolff, S., Higuchi, N., Santos, J. dos, Araujo, A. C. de, & Trumbore, S. (2017). A revised hydrological model for the Central Amazon: The importance of emergent canopy trees in the forest water budget. *Agricultural and Forest Meteorology*, *239*, 47–57. https://doi.org/10.1016/J.AGRFORMET.2017.03.002

Le Quéré, C., Andrew, R. M., Canadell, J. G., Sitch, S., Korsbakken, J. I., Peters, G. P., … Zaehle, S. (2016). Global Carbon Budget 2016. *Earth System Science Data*, *8*(2), 605–649. https://doi.org/10.5194/essd-8-605-2016

Lewis, S. L., Brando, P. M., Phillips, O. L., Van Der Heijden, G. M. F., & Nepstad, D. (2005). The 2010 Amazon Drought. https://doi.org/10.1126/science.1146961

Little, P. E. (2005). Indigenous Peoples and Sustainable Development Subprojects in Brazilian Amazonia: The Challenges of Interculturality. *Law & Policy*, *27*(3), 450–471. https://doi.org/10.1111/j.1467-9930.2005.00207.x

Liu, J., Bowman, K. W., Schimel, D. S., Parazoo, N. C., Jiang, Z., Lee, M., … Eldering, A. (2017). Contrasting carbon cycle responses of the tropical continents to the 2015–2016 El Niño. *Science*, *358*(6360). https://doi.org/10.1126/science.aam5690

Lohberger, S., Stängel, M., Atwood, E. C., & Siegert, F. (2018). Spatial evaluation of Indonesia's 2015 fire-affected area and estimated carbon emissions using Sentinel-1. *Global Change Biology*, *24*(2), 644–654. https://doi.org/10.1111/gcb.13841

Lüthi, D., Le Floch, M., Bereiter, B., Blunier, T., Barnola, J.-M., Siegenthaler, U., … Stocker, T. F. (2008). High-resolution carbon dioxide concentration record 650,000–800,000 years before present. *Nature*, *453*(7193), 379–382. https://doi.org/10.1038/nature06949

MacQueen, J., & others. (1967). Some methods for classification and analysis of multivariate observations. In *Proceedings of the fifth Berkeley symposium on mathematical statistics and probability* (Vol. 1, pp. 281–297).

Malhi, Y., Aragão, L. E. O. C., Galbraith, D., Huntingford, C., Fisher, R., Zelazowski, P., … Meir, P. (2009). Exploring the likelihood and mechanism of a climate-change-induced dieback of the Amazon rainforest. *Proceedings of the National Academy of Sciences of the United States of America*, *106*(49), 20610–20615. https://doi.org/10.1073/pnas.0804619106

Malhi, Y., Rowland, L., Aragão, L. E. O. C., & Fisher, R. A. (2018). New insights into the variability of the tropical land carbon cycle from the El Niño of 2015/2016. *Philosophical Transactions of the Royal Society B: Biological Sciences*, *373*(1760), 20170298. https://doi.org/10.1098/rstb.2017.0298

Malhi, Y., Wood, D., Baker, T. R., Wright, J., Phillips, O. L., Cochrane, T., … Vinceti, B. (2006). The regional variation of aboveground live biomass in old-growth

Amazonian forests. *Global Change Biology*, *12*(7), 1107–1138. https://doi.org/10.1111/j.1365-2486.2006.01120.x

Marengo, J. A., & Espinoza, J. C. (2016). Extreme seasonal droughts and floods in Amazonia: Causes, trends and impacts. *International Journal of Climatology*, *36*(3), 1033–1050. https://doi.org/10.1002/joc.4420

Marvin, D. C., Asner, G. P., Knapp, D. E., Anderson, C. B., Martin, R. E., Sinca, F., & Tupayachi, R. (2014). Amazonian landscapes and the bias in field studies of forest structure and biomass. *Proceedings of the National Academy of Sciences of the United States of America*, *111*(48), E5224-32. https://doi.org/10.1073/pnas.1412999111

McMichael, C. H., Piperno, D. R., Bush, M. B., Silman, M. R., Zimmerman, A. R., Raczka, M. F., … Silman, M. R. (2012). Sparse Pre-Columbian Human Habitation in Western Amazonia. *Science*, *336*(6087), 1429–1431. https://doi.org/10.1126/science.1219982

Mitchard, E. T. A. (2018). The tropical forest carbon cycle and climate change. *Nature*, *559*(7715), 527–534. https://doi.org/10.1038/s41586-018-0300-2

Nepstad, D. C., Stickler, C. M., Filho, B. S.-, & Merry, F. (2008). Interactions among Amazon land use, forests and climate: prospects for a near-term forest tipping point. *Philosophical Transactions of the Royal Society of London. Series B, Biological Sciences*, *363*(1498), 1737–1746. https://doi.org/10.1098/rstb.2007.0036

Nobre, C. A., & Borma, L. D. S. (2009). 'Tipping points' for the Amazon forest. *Current Opinion in Environmental Sustainability*, *1*(1), 28–36. https://doi.org/10.1016/J.COSUST.2009.07.003

Pachauri, R. K., Allen, M. R., Barros, V. R., Broome, J., Cramer, W., Christ, R., … others. (2014). *Climate change 2014: synthesis report. Contribution of Working Groups I, II and III to the fifth assessment report of the Intergovernmental Panel on Climate Change*. IPCC.

Palace, M., Keller, M., Asner, G. P., Silva, J. N. M., & Passos, C. (2007). Necromass in undisturbed and logged forests in the Brazilian Amazon. *Forest Ecology and Management*, *238*(1–3), 309–318. https://doi.org/10.1016/j.foreco.2006.10.026

Palace, M., Keller, M., Hurtt, G., & Frolking, S. (2012). A Review of Above Ground Necromass in Tropical Forests. *Tropical Forests*, 215–252. https://doi.org/10.5772/33085

Pan, Y., Birdsey, R. A., Fang, J., Houghton, R., Kauppi, P. E., Kurz, W. A., ... Hayes, D. (2011). A Large and Persistent Carbon Sink in the World's Forests. *Science*, *333*(6045), 988–993. https://doi.org/10.1126/science.1201609

Pan, Y., Birdsey, R. A., Phillips, O. L., & Jackson, R. B. (2013). The Structure, Distribution, and Biomass of the World's Forests. *Annual Review of Ecology, Evolution, and Systematics*, *44*(1), 593–622. https://doi.org/10.1146/annurev-ecolsys-110512-135914

Peres, C. A., Barlow, J., & Laurance, W. F. (2006). Detecting anthropogenic disturbance in tropical forests. *Trends in Ecology & Evolution*, *21*(5), 227–229. https://doi.org/10.1016/J.TREE.2006.03.007

Phillips, O. L., Aragão, L. E. O. C., Lewis, S. L., Fisher, J. B., Lloyd, J., López-González, G., ... others. (2009). Drought sensitivity of the Amazon rainforest. *Science*, *323*(5919), 1344–1347.

Pivello, V. R. (2011). The Use of Fire in the Cerrado and Amazonian Rainforests of Brazil: Past and Present. *Fire Ecology*, *7*(1), 24–39. https://doi.org/10.4996/fireecology.0701024

Power, M. J., Marlon, J., Ortiz, N., Bartlein, P. J., Harrison, S. P., Mayle, F. E., ... Zhang, J. H. (2008). Changes in fire regimes since the Last Glacial Maximum: an assessment based on a global synthesis and analysis of charcoal data. *Climate Dynamics*, *30*(7–8), 887–907. https://doi.org/10.1007/s00382-007-0334-x

Quesada, C. A., Phillips, O. L., Schwarz, M., Czimczik, C. I., Baker, T. R., Patiño, S., ... Lloyd, J. (2012). Basin-wide variations in Amazon forest structure and function are mediated by both soils and climate. *Biogeosciences*, *9*(6), 2203–2246. https://doi.org/10.5194/bg-9-2203-2012

Randerson, J. T., Chen, Y., van der Werf, G. R., Rogers, B. M., & Morton, D. C. (2012). Global burned area and biomass burning emissions from small fires. *Journal of Geophysical Research: Biogeosciences*, *117*(G4), n/a-n/a. https://doi.org/10.1029/2012JG002128

Ray, D., Nepstad, D., & Moutinho, P. (2005). MICROMETEOROLOGICAL AND CANOPY CONTROLS OF FIRE SUSCEPTIBILITY IN A FORESTED AMAZON LANDSCAPE. *Ecological Applications*, *15*(5), 1664–1678. https://doi.org/10.1890/05-0404

Rice, A. H., Pyle, E. H., Saleska, S. R., Hutyra, L., Palace, M., Keller, M., … Wofsy, S. C. (2004). CARBON BALANCE AND VEGETATION DYNAMICS IN AN OLD-GROWTH AMAZONIAN FOREST. *Ecological Applications*, *14*(sp4), 55–71. https://doi.org/10.1890/02-6006

Roosevelt, A. C. (2013). The Amazon and the Anthropocene: 13,000 years of human influence in a tropical rainforest. *Anthropocene*, *4*, 69–87. https://doi.org/10.1016/J.ANCENE.2014.05.001

Saatchi, S., Houghton, R. A., Dos Santos Alvalá, R. C., Soares, J. V., & Yu, Y. (2007). Distribution of aboveground live biomass in the Amazon basin. *Global Change Biology*, *13*(4), 816–837. https://doi.org/10.1111/j.1365-2486.2007.01323.x

Saatchi, S. S., Harris, N. L., Brown, S., Lefsky, M., Mitchard, E. T. A., Salas, W., … Morel, A. (2011). Benchmark map of forest carbon stocks in tropical regions across three continents. *Proceedings of the National Academy of Sciences*, *108*(24), 9899–9904. https://doi.org/10.1073/pnas.1019576108

Saatchi, S. S., Houghton, R. A., Dos Santos Alvalá, R. C., Soares, J. V., & Yu, Y. (2007). Distribution of aboveground live biomass in the Amazon basin. *Global Change Biology*, *13*(4), 816–837. https://doi.org/10.1111/j.1365-2486.2007.01323.x

Schöngart, J., Junk, W. J., Piedade, M. T. F., Ayres, J. M., Hüttermann, A., & Worbes, M. (2004). Teleconnection between tree growth in the Amazonian floodplains and the El Niño-Southern Oscillation effect. *Global Change Biology*, *10*(5), 683–692. https://doi.org/10.1111/j.1529-8817.2003.00754.x

Silva, C. V. J., Aragão, L. E. O. C., Barlow, J., Espirito-Santo, F., Young, P. J., Anderson, L. O., … Xaud, H. A. M. (2018). Drought-induced Amazonian wildfires instigate a decadal-scale disruption of forest carbon dynamics. *Philosophical Transactions of the Royal Society B: Biological Sciences*, *373*(1760), 20180043. https://doi.org/10.1098/rstb.2018.0043

Slik, J. W. F., Arroyo-Rodríguez, V., Aiba, S.-I., Alvarez-Loayza, P., Alves, L. F., Ashton, P., … Venticinque, E. M. (2015). An estimate of the number of tropical tree

species. *Proceedings of the National Academy of Sciences of the United States of America*, *112*(24), 7472–7477. https://doi.org/10.1073/pnas.1423147112

Soares-Filho, B., Moutinho, P., Nepstad, D., Anderson, A., Rodrigues, H., Garcia, R., … Maretti, C. (2010). Role of Brazilian Amazon protected areas in climate change mitigation. *Proceedings of the National Academy of Sciences*, *107*(24), 10821–10826. https://doi.org/10.1073/pnas.0913048107

Spracklen, D. V., & Garcia-Carreras, L. (2015). The impact of Amazonian deforestation on Amazon basin rainfall. *Geophysical Research Letters*, *42*(21), 9546–9552. https://doi.org/10.1002/2015GL066063

Strand, J., Soares-Filho, B., Costa, M. H., Oliveira, U., Ribeiro, S. C., Pires, G. F., … Toman, M. (2018). Spatially explicit valuation of the Brazilian Amazon Forest's Ecosystem Services. *Nature Sustainability*, *1*(11), 657–664. https://doi.org/10.1038/s41893-018-0175-0

Thornton, P. K., Ericksen, P. J., Herrero, M., & Challinor, A. J. (2014). Climate variability and vulnerability to climate change: a review. *Global Change Biology*, *20*(11), 3313–3328. https://doi.org/10.1111/gcb.12581

Timmermann, A., Oberhuber, J., Bacher, A., Esch, M., Latif, M., & Roeckner, E. (1999). Increased El Niño frequency in a climate model forced by future greenhouse warming. *Nature*, *398*(6729), 694–697. https://doi.org/10.1038/19505

Tudhope, A. W., Chilcott, C. P., McCulloch, M. T., Cook, E. R., Chappell, J., Ellam, R. M., … Shimmield, G. B. (2001). Variability in the El Niño-Southern Oscillation through a glacial-interglacial cycle. *Science (New York, N.Y.)*, *291*(5508), 1511–1517. https://doi.org/10.1126/science.1057969

Turcq, B., Sifeddine, A., Martin, L., Absy, M. L., Soubies, F., Suguio, K., & Volkmer-Ribeiro, C. (1998). Amazonia rainforest fires: a lacustrine record of 7000 years. *Ambio*, *27*(2), 139–142. https://doi.org/10.2307/4314700

Uhl, C., & Kauffman, J. B. (1990). Deforestation, Fire Susceptibility, and Potential Tree Responses to Fire in the Eastern Amazon. *Ecology*, *71*(2), 437–449. https://doi.org/10.2307/1940299

USGS. (2016). *LANDSAT SURFACE REFLECTANCE-DERIVED SPECTRAL INDICES.*

USGS. https://doi.org/10.1080/1073161X.1994.10467258

van der Laan-Luijkx, I. T., van der Velde, I. R., Krol, M. C., Gatti, L. V., Domingues, L. G., Correia, C. S. C., … Peters, W. (2015). Response of the Amazon carbon balance to the 2010 drought derived with CarbonTracker South America. *Global Biogeochemical Cycles*, *29*(7), 1092–1108. https://doi.org/10.1002/2014GB005082

van der Werf, G. R., Randerson, J. T., Giglio, L., van Leeuwen, T. T., Chen, Y., Rogers, B. M., … Kasibhatla, P. S. (2017). Global fire emissions estimates during 1997–2016. *Earth System Science Data*, *9*(2), 697–720. https://doi.org/10.5194/essd-9-697-2017

van Leeuwen, T. T., van der Werf, G. R., Hoffmann, A. A., Detmers, R. G., Rücker, G., French, N. H. F. F., … Trollope, W. S. W. W. (2014). Biomass burning fuel consumption rates: A field measurement database. *Biogeosciences*, *11*(24), 7305–7329. https://doi.org/10.5194/bg-11-7305-2014

Wang, W., Ciais, P., Nemani, R. R., Canadell, J. G., Piao, S., Sitch, S., … Myneni, R. B. (2013). Variations in atmospheric CO2 growth rates coupled with tropical temperature. *Proceedings of the National Academy of Sciences of the United States of America*, *110*(32), 13061–13066. https://doi.org/10.1073/pnas.1219683110

Yang, Y., Saatchi, S. S., Xu, L., Yu, Y., Choi, S., Phillips, N., … Myneni, R. B. (2018). Post-drought decline of the Amazon carbon sink. *Nature Communications*, *9*(1), 3172. https://doi.org/10.1038/s41467-018-05668-6

9 APPENDICES

APPENDIX 1 TABLE OF INPUT DATA USED TO PRODUCE LAND-USE AND BURNED AREA MAP

Table 3. Landsat scenes, dates, and products used as input data to the k-mean unsupervised classification used to classify land-uses between 2010 and 2017 in central-eastern Amazonia. NDVI = Normalised Difference Vegetation Index; SAVI = Soil-Adjusted Vegetation Index; EVI = Enhanced Vegetation Index; NBR2 = Normalised Burn Ratio 2 (USGS, 2016).

Path/Row	Sensor/mission	Date	Products
227/062	Landsat 5 TM	31/07/2010	Bands 1-7; NDVI; SAVI; EVI; NBR2
227/062	Landsat 5 TM	16/06/2011	Bands 1-7; NDVI; SAVI; EVI; NBR2
227/062	Landsat 7 ETM+	28/07/2012	Bands 1-8
227/062	Landsat 7 ETM+	14/09/2012	Bands 1-8
227/062	Landsat 7 ETM+	17/11/2012	Bands 1-8
227/062	Landsat 8 OLI	25/09/2013	Bands 2-8; NDVI; SAVI; EVI; NBR2
227/062	Landsat 8 OLI	30/08/2014	Bands 2-8; NDVI; SAVI; EVI; NBR2
227/062	Landsat 8 OLI	30/10/2014	Bands 2-8; NDVI; SAVI; EVI; NBR2
227/062	Landsat 8 OLI	02/01/2015	Bands 2-8; NDVI; SAVI; EVI; NBR2
227/062	Landsat 8 OLI	29/07/2015	Bands 2-8; NDVI; SAVI; EVI; NBR2
227/062	Landsat 8 OLI	29/06/2016	Bands 2-8; NDVI; SAVI; EVI; NBR2
227/062	Landsat 8 OLI	16/08/2016	Bands 2-8; NDVI; SAVI;

			EVI; NBR2
227/063	Landsat 5 TM	31/07/2010	Bands 1-7; NDVI; SAVI; EVI; NBR2
227/063	Landsat 5 TM	16/06/2011	Bands 1-7; NDVI; SAVI; EVI; NBR2
227/063	Landsat 7 ETM+	28/07/2012	Bands 1-8
227/063	Landsat 7 ETM+	14/09/2012	Bands 1-8
227/063	Landsat 7 ETM+	30/09/2012	Bands 1-8
227/063	Landsat 8 OLI	25/09/2013	Bands 2-8; NDVI; SAVI; EVI; NBR2
227/063	Landsat 8 OLI	10/07/2014	Bands 2-8; NDVI; SAVI; EVI; NBR2
227/063	Landsat 8 OLI	23/03/2015	Bands 2-8; NDVI; SAVI; EVI; NBR2
227/063	Landsat 8 OLI	27/06/2015	Bands 2-8; NDVI; SAVI; EVI; NBR2
227/063	Landsat 8 OLI	29/07/2015	Bands 2-8; NDVI; SAVI; EVI; NBR2
227/063	Landsat 8 OLI	31/07/2016	Bands 2-8; NDVI; SAVI; EVI; NBR2
227/063	Landsat 8 OLI	16/08/2016	Bands 2-8; NDVI; SAVI; EVI; NBR2
228/062	Landsat 5 TM	22/07/2010	Bands 1-7; NDVI; SAVI; EVI; NBR2
228/062	Landsat 5 TM	07/06/2011	Bands 1-7; NDVI; SAVI; EVI; NBR2
228/062	Landsat 7 ETM+	21/09/2012	Bands 1-8
228/062	Landsat 7 ETM+	23/10/2012	Bands 1-8

228/062	Landsat 7 ETM+	24/11/2012	Bands 1-8
228/062	Landsat 8 OLI	16/09/2013	Bands 2-8; NDVI; SAVI; EVI; NBR2
228/062	Landsat 8 OLI	15/08/2013	Bands 2-8; NDVI; SAVI; EVI; NBR2
228/062	Landsat 8 OLI	15/06/2014	Bands 2-8; NDVI; SAVI; EVI; NBR2
228/062	Landsat 8 OLI	17/05/2015	Bands 2-8; NDVI; SAVI; EVI; NBR2
228/062	Landsat 8 OLI	02/06/2015	Bands 2-8; NDVI; SAVI; EVI; NBR2
228/062	Landsat 8 OLI	18/06/2015	Bands 2-8; NDVI; SAVI; EVI; NBR2
228/062	Landsat 8 OLI	07/08/2016	Bands 2-8; NDVI; SAVI; EVI; NBR2
228/062	Landsat 8 OLI	24/09/2016	Bands 2-8; NDVI; SAVI; EVI; NBR2
228/063	Landsat 5 TM	22/07/2010	Bands 1-7; NDVI; SAVI; EVI; NBR2
228/063	Landsat 5 TM	10/08/2011	Bands 1-7; NDVI; SAVI; EVI; NBR2
228/063	Landsat 7 ETM+	20/08/2012	Bands 1-8
228/063	Landsat 7 ETM+	23/10/2012	Bands 1-8
228/063	Landsat 7 ETM+	10/12/2012	Bands 1-8
228/063	Landsat 8 OLI	28/06/2013	Bands 2-8; NDVI; SAVI; EVI; NBR2
228/063	Landsat 8 OLI	15/06/2014	Bands 2-8; NDVI; SAVI; EVI; NBR2

228/063	Landsat 8 OLI	17/05/2015	Bands 2-8; NDVI; SAVI; EVI; NBR2
228/063	Landsat 8 OLI	20/07/2015	Bands 2-8; NDVI; SAVI; EVI; NBR2
228/063	Landsat 8 OLI	06/07/2016	Bands 2-8; NDVI; SAVI; EVI; NBR2
228/063	Landsat 8 OLI	07/08/2016	Bands 2-8; NDVI; SAVI; EVI; NBR2

APPENDIX 2 PUBLISHED VERSION OF THE MANUSCRIPT

Quantifying immediate carbon emissions from El Niño-mediated wildfires in humid tropical forests

Kieran Withey[1], Erika Berenguer[1,2], Alessandro Ferraz Palmeira[3], Fernando D. B. Espírito-Santo[4], Gareth D. Lennox[1], Camila V. J. Silva[1], Luiz E. O. C. Aragão[5,6], Joice Ferreira[7], Filipe França[1,7,8], Yadvinder Malhi[2], Liana Chesini Rossi[9] and Jos Barlow[1]

[1]Lancaster Environment Centre, Lancaster University, Lancaster LA1 4YQ, UK
[2]Environmental Change Institute, University of Oxford, Oxford OX1 3QY, UK
[3]Instituto de Ciências Biológicas, Universidade Federal do Pará, Rua Augusto Corrêa, 01, Campus Guamá, Belém, PA CEP: 66075-110, Brazil
[4]Centre for Landscape and Climate Research (CLCR) and Leicester Institute of Space and Earth Observation (LISEO), School of Geography, Geology and Environment, University of Leicester, University Road, Leicester LE1 7RH, UK
[5]Remote Sensing Division, National Institute for Space Research, Avenida dos Astronautas, 1.758, 12227-010 São José dos Campos, São Paulo, Brazil
[6]College of Life and Environmental Sciences, University of Exeter, Exeter EX4 4RJ, UK
[7]Embrapa Amazônia Oriental, Travessa Dr Enéas Pinheiro, s/n, CP 48, 66095-100 Belém, Pará, Brazil
[8]Instituto Federal de Minas Gerais, Rodovia Bambuí/Medeiros, Km-05, 38900-000 Bambuí, Minas Gerais, Brazil
[9]Departamento de Ecologia, Universidade Estadual Paulista, 13506-900 Rio Claro, São Paulo, Brazil

KW, 0000-0002-9550-4249; EB, 0000-0001-8157-8792

Wildfires produce substantial CO_2 emissions in the humid tropics during El Niño-mediated extreme droughts, and these emissions are expected to increase in coming decades. Immediate carbon emissions from uncontrolled wildfires in human-modified tropical forests can be considerable owing to high necromass fuel loads. Yet, data on necromass combustion during wildfires are severely lacking. Here, we evaluated necromass carbon stocks before and after the 2015–2016 El Niño in Amazonian forests distributed along a gradient of prior human disturbance. We then used Landsat-derived burn scars to extrapolate regional immediate wildfire CO_2 emissions during the 2015–2016 El Niño. Before the El Niño, necromass stocks varied significantly with respect to prior disturbance and were largest in undisturbed primary forests (30.2 ± 2.1 Mg ha^{-1}, mean $\pm$ s.e.) and smallest in secondary forests (15.6 ± 3.0 Mg ha^{-1}). However, neither prior disturbance nor our proxy of fire intensity (median char height) explained necromass losses due to wildfires. In our 6.5 million hectare (6.5 Mha) study region, almost 1 Mha of primary (disturbed and undisturbed) and 20 000 ha of secondary forest burned during the 2015–2016 El Niño. Covering less than 0.2% of Brazilian Amazonia, these wildfires resulted in expected immediate CO_2 emissions of approximately 30 Tg, three to four times greater than comparable estimates from global fire emissions databases. Uncontrolled understorey wildfires in humid tropical forests during extreme droughts are a large and poorly quantified source of CO_2 emissions.

This article is part of a discussion meeting issue 'The impact of the 2015/2016 El Niño on the terrestrial tropical carbon cycle: patterns, mechanisms and implications'.

1. Introduction

Increased concentrations of atmospheric CO_2 during El Niño Southern Oscillation events [1,2] have largely been attributed to emissions from the tropics [3,4], with wildfires playing an important role [4,5]. In recent decades, despite a global

Table 1. Forest classifications for pre-El Niño forest disturbance classes and the plot samples in 2010, 2014–2015 and 2017. The 2015–2016 sample occurred after extensive wildfires and is a subset of the 2014–2015 sample.

pre-El Niño forest class	definition	necromass assessment (2010)	monitoring of CWD (2014–2015)	burned in 2015–2016 and sampled in 2017	additionally burned area sampling (2017)
undisturbed primary forest	primary forest with no evidence of human disturbance, such as fire scars or logging stumps	17	5	2	3
logged primary forest	primary forest with evidence of logging, such as logging stumps	26	5	4	1
burned primary forest	primary forest with evidence of recent fire, such as fire scars	7	0	0	0
logged-and-burned primary forest	primary forest with evidence of both logging and fire	24	4	1	4
secondary forest	forest regenerating after complete removal of native vegetation	33	4	0	1

reduction in burned vegetation area [6,7], relatively low-intensity understorey wildfires that spread from agricultural lands have increased in the fire-sensitive Amazon rainforest [8–11]. CO_2 emissions from such wildfires are expected to grow further [10] as fire-conducive weather patterns increase across the humid tropics, particularly in South America [12].

Large-scale understorey wildfires in Amazonia are unprecedented in recent millennia. During pre-Columbian times, fires were limited to those occurring naturally from lightning strikes and prescribed burns by indigenous peoples [13]. These fires were localized and prescribed burns were planned in accordance with environmental and ecological conditions [13]. However, pervasive human modification of tropical forest landscapes, through, for example, road building, cattle ranching and timber exploitation, combined with severe drought events and the widespread use of fire as a land management tool, has fundamentally altered Amazonian fire regimes. Today, uncontrolled large-scale understorey wildfires are being witnessed in the Amazon with sub-decadal frequency [14]. Such wildfires result in high rates of tree mortality [15,16], shifts in forest structure [17,18] and drier microclimatic conditions [19], ultimately leading to increased susceptibility to future wildfires [19–21].

Carbon emissions from understorey wildfires can be split into committed and immediate emissions. Committed emissions result from the complex interplay between delayed tree mortality and decomposition, and are dependent on future climatic conditions and human influences. Research indicates that long-term storage of carbon in wildfire-affected Amazonian forests can be compromised for decades: even 31 years after a fire event, burned forests store approximately 25% less carbon than unburned control sites owing to high levels of tree mortality that are not compensated by regrowth [22]. Immediate understorey emissions are those that occur during wildfires and, in contrast to committed emissions, are relatively simple to estimate. Biome- and continent-wide analyses that rely on satellite observations (known as top-down studies) suggest that these immediate emissions from tropical forests can be substantial [23,24] and, for example, can transform the

Amazon basin from a carbon sink to a large carbon source during drought years [25].

One potentially important source of immediate carbon emissions during wildfires is dead organic matter found on forest floors. This necromass, which includes leaf litter and woody debris, is a fundamental component of forest structure and dynamics and can account for up to 40% of the carbon stored in humid tropical forests [26–28]. During long periods of drought, this large carbon pool can become highly flammable [29]. However, studies quantifying necromass stocks have overwhelmingly focused on undisturbed primary forests [27]; studies that estimate necromass in human-modified tropical forests—forests that have been structurally altered by anthropogenic disturbance, such as selective logging and fires, and those regenerating following deforestation (commonly called *secondary forests*; table 1)—are rare (cf. [30,31]). This represents a key gap in our understanding because human-modified tropical forests are increasingly prevalent [32] and increasingly vulnerable to wildfires [33–35]. While many local-scale, bottom-up studies have quantified combustion characteristics and carbon emissions following fires related to deforestation and slash-and-burn practices (see Van Leeuwen *et al.* [36] for a recent review), we know of no study that quantifies necromass before and after uncontrolled understorey wildfires in human-modified Amazonian forests. These knowledge gaps and data shortfalls limit our understanding of immediate carbon emissions from understorey wildfires. Improving such estimates is essential for refining Earth Systems models and both national and global estimates of greenhouse gas emissions.

Here, we address these knowledge gaps using a hybrid bottom-up/top-down approach to study a human-modified region of central-eastern Amazonia that experienced almost 1 million hectares (1 Mha) of understorey wildfires during the 2015–2016 El Niño (figure 1). We combine data from a previously published large-scale field assessment of carbon stocks [37] with on-the-ground measures of woody debris before and after the 2015–2016 El Niño, proxies of fire intensity and coverage within study plots, and remotely sensed analyses of fire extent across the region. Specifically, we (a) quantify carbon
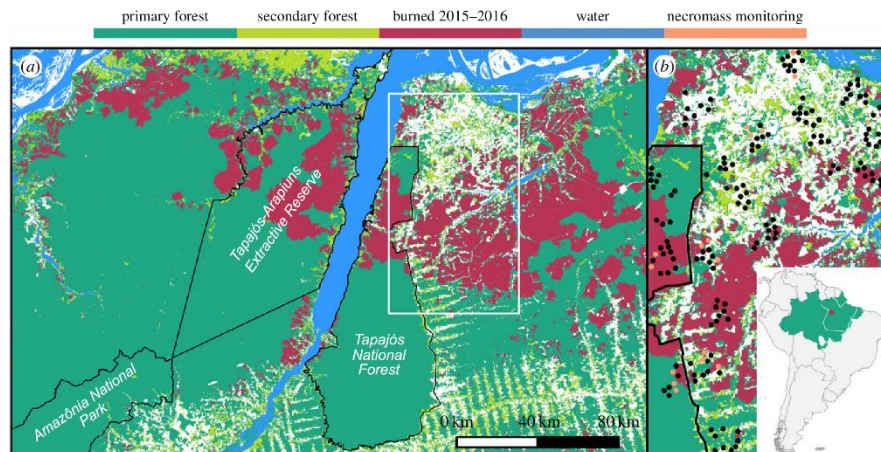
Kieran Daniel Withey - March 2019

Figure 1. (*a*) The 2017 land-use map across the approximately 6.5 Mha study region. (*b*) The land-use map within the RAS study area (shown by the white border in (*a*)). Also shown in this panel are the locations of the 107 study plots (black circles). The 18 of these that were used for necromass monitoring are shown as orange circles. The inset shows the Santarém study region (red circle) within South America, the Brazilian Amazon (green) and Pará (white border).

stocks vulnerable to combustion across human-modified tropical forests in central-eastern Amazonia, (b) use post-burn measures to investigate the factors influencing the loss of necromass during wildfires, (c) estimate region-wide immediate carbon emissions from wildfires and (d) compare these region-wide emission estimates with those derived from widely used global fire emissions databases.

2. Methods

(a) Quantifying necromass stocks in human-modified Amazonian forests

We established 107 plots (0.25 ha) in human-modified forests in central-eastern Amazonia in 2010 (figure 1). Plots were located in the municipalities of Santarém, Belterra and Mojuí dos Campos in the state of Pará, Brazil, and form part of the Sustainable Amazon Network (*Rede Amazônia Sustentável* (RAS) in Portuguese [38]). Study plots covered a range of prior human impacts (table 1) and included undisturbed primary forests ($n = 17$), primary forests selectively logged prior to 2010 ($n = 26$), primary forests burned prior to 2010 ($n = 7$), primary forests logged and burned prior to 2010 ($n = 24$) and secondary forests recovering after complete removal of vegetation ($n = 33$; table 1).

Summary carbon estimates for these 107 plots can be found in Berenguer *et al.* [37]. Here, we focused on carbon stored in their necromass pools. We estimated necromass stocks in dead-standing tree and palm stems, coarse woody debris (CWD; ≥ 10 cm diameter at one extremity), fine woody debris (FWD; ≥ 2 and <10 cm diameter at both extremities) and leaf litter (including twigs <2 cm diameter at both extremities, leaves, and fruits and seeds). Full carbon estimation methods can be found in Berenguer *et al.* [37]. In brief, in each plot, we measured the diameter and height of all large (greater than or equal to 10 cm diameter at breast height (DBH)) dead tree and palm stems. We measured the diameter and height of all small dead tree and palm stems (≥ 2 and <10 DBH) in five subplots (5×20 m) in each plot. We used the allometric equations of Hughes *et al.* [39] and Cummings *et al.* [40] to estimate, respectively, carbon stocks for dead-standing trees and palms. Subplots were also

used to estimate the diameters and lengths of all pieces of fallen CWD. We estimated the volume of each piece of CWD using Smalian's formula [27] after accounting for the extent of damage (i.e. void space). We multiplied the volume of each CWD piece by its decomposition class to calculate CWD mass [30]. In all study plots, we established five smaller subplots (2×5 m) to assess FWD. This was sampled and weighed in the field. A subsample (≤ 1 kg) was collected in each subplot and oven-dried to a constant weight. The wet-to-dry ratios of the FWD samples were used to estimate the total FWD stocks per plot. To estimate the biomass of leaf litter, ten 0.5×0.5 m quadrats were established in each plot. We oven-dried leaf litter samples to a constant weight to get an estimate of the leaf litter stocks in each plot. Biomass estimates for each necromass component were then standardized to per hectare values, and the carbon content was assumed to be 50% of biomass dry weight [41]. See electronic supplementary materials (§1) for all equations we used to estimate necromass biomass.

(b) Longitudinal monitoring of coarse woody debris

To estimate necromass change through time, we continued to monitor 18 of the 107 RAS plots (figure 1). These 18 plots were chosen because they are spatially distributed across the region and we were able to secure long-term authorization to monitor them. They included undisturbed primary forests ($n = 5$), primary forests logged prior to 2010 ($n = 5$), primary forest logged and burned prior to 2010 ($n = 4$), and secondary forests ($n = 4$; table 1). We conducted surveys of the 18 plots between November 2014 and September 2015, using a slightly altered sampling design to align with the Global Ecosystem Monitoring protocol (see [42] for details). We established five 1×20 m subplots in each of the 18 plots, measured all pieces of CWD, and estimated their biomass and carbon content following the methods outlined above (see Methods (a)).

(c) Impacts of El Niño-mediated wildfires on necromass stocks

Extensive understorey wildfires burned seven of our 18 study plots during the 2015–2016 El Niño, including two previously undisturbed primary forests, four primary forests logged prior to

2010, and one primary forest that was logged and burned prior to 2010. To investigate necromass carbon stock losses due to these wildfires, we resurveyed all 18 plots in June 2017. We re-measured each individual piece of CWD and estimated biomass using the methods described above (Methods (a)). By comparing CWD stocks before and after the El Niño in the 11 plots that did not experience wildfires, we were able to estimate CWD background decomposition rates. By comparing CWD stocks before and after the El Niño in the seven plots that burned, we were able to measure CWD combustion completeness.

We used values from the 2010 surveys to provide estimates of the pre-El Niño carbon stocks in leaf litter and FWD. Based on visual inspection of the sites (electronic supplementary material, figure S1), we assumed 100% combustion completeness of these necromass components in the fire-affected proportion of burned plots. Recognizing that this is a strong assumption, we consider the validity of it in our Discussion. We did not consider wildfire-mediated changes in necromass carbon stocks in dead-standing trees and palms, owing to a lack of data on combustion completeness.

In the seven plots that burned, we calculated average char height for each stem, defined as the sum of the maximum and minimum char heights divided by two. We then used these average stem char heights to calculate the plot-level median char height, which we used as our proxy for fire intensity. In addition, we used the proportion of sampled stems with burn scars as an estimate of the area of each plot that burned (electronic supplementary materials). To increase our sample of fire-affected plots (to 16), we also estimated the area burned in an additional nine of the original RAS plots that were sampled during the 2010 censuses and burned during 2015–2016 (table 1). Prior to the wildfires, these additional plots included undisturbed primary forests ($n = 3$), primary forests logged prior to 2010 ($n = 1$), primary forests logged and burned prior to 2010 ($n = 4$), and secondary forests ($n = 1$).

We used these data to estimate the per hectare necromass loss (NL) attributable to wildfires using the following equation:

$$NL = FL_{CWD} \times (CC_{CWD} - D_{CWD}) + FL_{LLFWD} \times BA, \qquad (2.1)$$

where FL_{CWD} is the per hectare fuel load of CWD estimated from the 107 RAS plots surveyed in 2010, CC_{CWD} is the combustion completeness of CWD estimated from seven of the 18 CWD monitoring plots that burned during the 2015–2016 El Niño, D_{CWD} is the background CWD decomposition rate estimated from the 11 CWD monitoring plots that did not burn during the 2015–2016 El Niño, FL_{LLFWD} is the per hectare fuel load of leaf litter and FWD estimated from the 107 plots surveyed in 2010, and BA is the proportion of the plot that burned estimated from the 16 RAS plots that burned (seven necromass monitoring sites and nine additional sites in which burned area was estimated) during the 2015–2016 El Niño (table 1).

(d) Data analysis

We used the Kruskal–Wallis test to investigate variation across forest classes of prior human disturbance (table 1) and used the Conover–Iman test with Bonferroni adjustments to perform multiple pairwise comparisons of forest class medians. We assessed differences across forest classes in: carbon stocks stored in each necromass component (i.e. dead-standing stems, CWD, FWD and leaf litter) from the 2010 survey; total and percentage necromass carbon stock losses in the 18 plots surveyed between 2014 and 2017; and the proportion/area of plots burned during the 2015–2016 El Niño. We used linear regression to investigate the relationship between: necromass carbon stocks before and after the 2015–2016 El Niño; fire intensity and stock losses; and the burned area in each plot and stock losses.

(e) Estimating burned area and region-wide emissions from forest fires

To estimate wildfire-mediated carbon emissions from necromass across our study region, we first calculated the cumulative area of primary and secondary forest that experienced understorey wildfires during 2015–2016 in the central-eastern region of the Amazon, an area of approximately 6.5 Mha (figure 1). We built a time-series of Landsat (5, 7 and 8) imagery from 2010 to 2017 for the RAS study region and the surrounding area from the EROS Science Processing Architecture (ESPA)/U.S. Geological Survey (USGS) website (https://espa.cr.usgs.gov). We performed an unsupervised classification of raw imagery, followed by manual correction of classification errors, to identify several land-uses throughout the time-series (see electronic supplementary material, table S2 for all land-use classes and §2 for a detailed description of burned area detection). We then used the burned area of primary and secondary forests and estimates of per hectare necromass stock losses from wildfires (equation (2.1)) to determine region-wide necromass carbon emissions, using a conversion factor of 3.286 kg of CO_2 per kg of C [43]. This conversion factor does not include other forms of emitted C (such as CO), in keeping with global fire emissions databases.

We took two approaches to account for uncertainty in expected regional necromass emissions. First, we considered four land-use scenarios using two sets of primary and secondary forests (electronic supplementary material, table S1). To account for potential variation in fire susceptibility across primary forest disturbance classes, we estimated the five variables in equation (2.1) using all undisturbed and disturbed primary forest classes (prim1) and then only disturbed primary forests (prim2). For secondary forests, we used CC_{CWD} and FL_{LLFWD} from all secondary forests, used D_{CWD} and BA from all forest classes combined, and used CC_{CWD} from all primary forest classes because none of the secondary forest plots we were monitoring for changes in CWD burned during 2015–2016 (sec1). Our other scenario for secondary forests (sec2) was more restrictive: we used the fuel load (FL_{CWD}, FL_{LLFWD}), decomposition (D_{CWD}), and BA values from secondary forests only and combined these with all CC_{CWD} values we had from disturbed and undisturbed primary forests.

Second, to account for uncertainty in the distribution of the variables in equation (2.1), we ran 1000 bootstrap with replacement simulations to determine each variable's mean value and standard error. We calculated the standard error of equation (2.1) using the variable standard errors, accounting for error propagation, and we constructed 95% confidence intervals for equation (2.1) as its mean value ± 1.96 times the standard error of the mean.

(f) Emissions and burned area comparisons with global databases

We compared our region-wide CO_2 emission estimates with two fire emissions databases frequently used in Earth Systems models and carbon budgets: the Global Fire Emissions Database (GFED) version 4.1s [44] and the Global Fire Assimilation System (GFAS) version 1.1 [45]. For both datasets, we obtained data for our study period (August 2015–July 2016) and cropped them to our approximately 6.5 Mha study region, shown in figure 1.

We first calculated cumulative emissions from GFED and GFAS (electronic supplementary material) and compared these with our emissions estimates. Second, to investigate potential sources of discrepancy between estimates, we spatially mapped GFED, GFAS and our CO_2 emissions estimates. At both GFED and GFAS resolutions (0.25° and 0.1°, respectively), we mapped our mean (across land-use scenarios; electronic supplementary material, table S1) expected emissions assuming that emissions were constant in a burned area (i.e. if a cell contained x% of the burned area, we assumed it accounted for x% of the total emissions). Finally, because
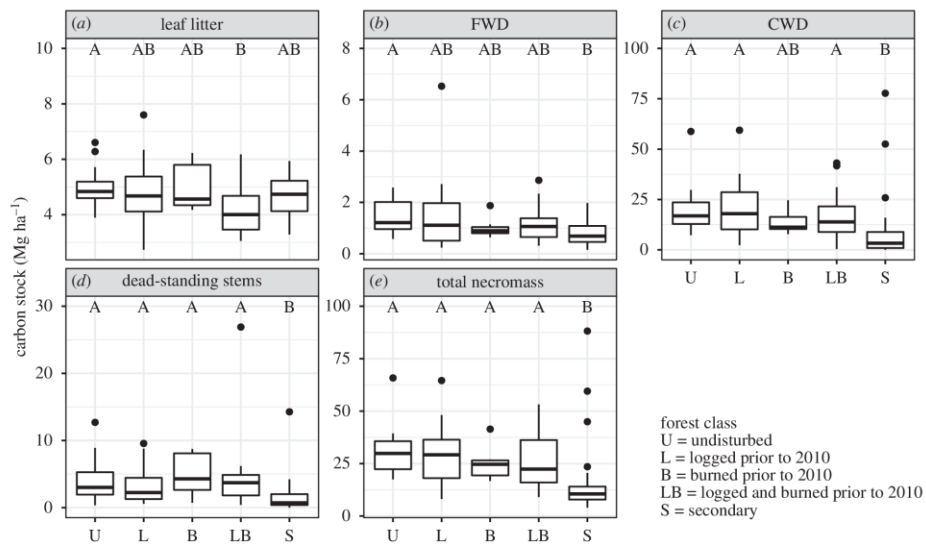
Kieran Daniel Withey - March 2019

Figure 2. Necromass carbon stocks in leaf litter (*a*), FWD (*b*), CWD (*c*) and dead standing stems (*d*), and the total across all components (*e*) in human-modified Amazonian forests. Boxplots show the interquartile range. Letters above the boxplots show the results from multiple pairwise comparisons of forest class medians. Classes that do not share a letter have significantly different medians ($p < 0.05$).

GFED also provides estimates of the area burned at 0.25°, we used our land-use map to estimate burned area at that resolution.

3. Results

(a) Necromass carbon stocks across human-modified Amazonian forests

Total necromass and its components varied significantly with respect to forest class ($p < 0.05$ in all cases; figure 2). Primary forests contained significantly higher total necromass than secondary forests ($p < 0.01$ for all pairwise comparisons), with the highest total found in undisturbed primary forests (30.2 $\pm$ 2.1 Mg ha^{-1}, mean $\pm$ s.e.). By contrast, secondary forests contained only half as much necromass as undisturbed primary forests (15.6 $\pm$ 3.0 Mg ha^{-1}). Variation in total necromass was driven in large part by variation in CWD, which accounted for 61.3 $\pm$ 2.7% of the total necromass stocks across forest classes. Leaf litter was the next most important component of total necromass, with 19.8 $\pm$ 2.7% residing in this component. Dead-standing stems accounted for 14.4 $\pm$ 1.8% of total necromass. Finally, FWD was by far the smallest necromass component, harbouring just 4.6 $\pm$ 0.2% of the total.

(b) Impacts of El Niño-mediated wildfires on necromass stocks

On average, we estimate that 87.1 $\pm$ 2.7% of the ground area of our fire-affected study plots burned, and there was no significant difference in the total burned area of fire-affected plots across forest classes ($\chi_3^2 = 2.1$; $p = 0.56$). From the 88 CWD pieces measured before the fires, 54 completely burned, 32 had partial combustion, and two were untouched by fire. CWD carbon stock losses from combustion varied from 38 to 94% (mean 65.4%, s.e. 7.1%) at the plot-level.

Necromass carbon stock losses in the seven burned plots were unrelated to median char height ($R^2 = 0.09$; $p = 0.51$; figure 3*a*) and area of plot burned ($R^2 = 0.10$; $p = 0.49$; figure 3*b*). Forest class did not predict necromass carbon stock losses in burned sites when expressed as either percentage ($\chi_2^2 = 2.25$; $p = 0.32$) or total ($\chi_2^2 = 1.12$; $p = 0.57$) loss. Similarly, forest class did not predict necromass losses in unburned sites when expressed as either percentage ($\chi_3^2 = 1.58$; $p = 0.66$) or total ($\chi_3^2 = 2.18$; $p = 0.54$) loss.

On average, burned sites lost 73.0 $\pm$ 4.9% of their pre-El Niño necromass stocks (figure 4), compared with a 26.1 $\pm$ 4.8% reduction in unburned sites (from decomposition). As expected, pre-El Niño necromass stocks strongly predicted post-El Niño necromass in our unburned sites ($R^2 = 0.95$; $p < 0.001$; figure 4*a*). This relationship disappeared in fire-affected plots ($R^2 = 0.08$; $p = 0.54$; figure 4*b*), indicating that combustion completeness was insensitive to initial necromass stocks. Despite our small sample size, visual inspection suggests that these findings were unaffected by forest class.

(c) Region-wide burned area and estimates of carbon stock losses

During the 2015–2016 El Niño, 15.2% of our study region and 982 276 ha of forest experienced understorey wildfires. These wildfires were overwhelmingly concentrated in primary forests: less than 2% of the burned area was in secondary forests, despite these accounting for 9% of the forest cover in our study region. When considering all primary and secondary forest plots (prim1 + sec1), resultant necromass carbon stock losses amounted to 10.06 Tg (95% confidence interval, 5.85–14.27 Tg). Converting to CO_2, this is equivalent to expected emissions of 33.05 Tg (95% confidence interval, 19.22–46.87 Tg; figure 5). Our mean CO_2 emission estimates were relatively insensitive to the
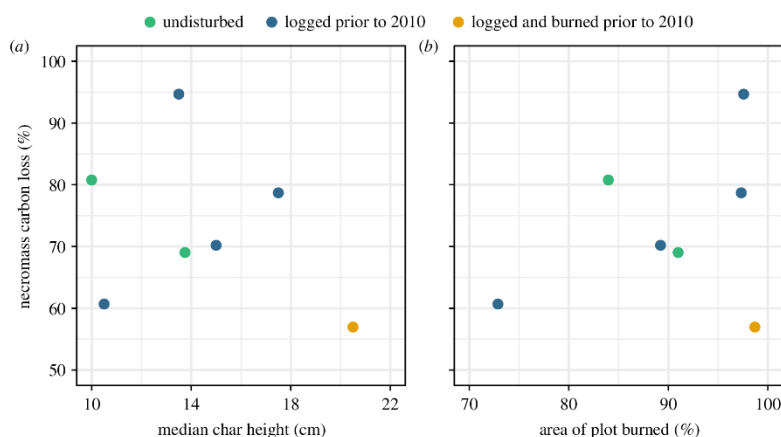
Figure 3. (*a*) Necromass carbon stock losses and fire intensity, as measured by median char height. (*b*) Necromass carbon stock losses and area of plot burned.
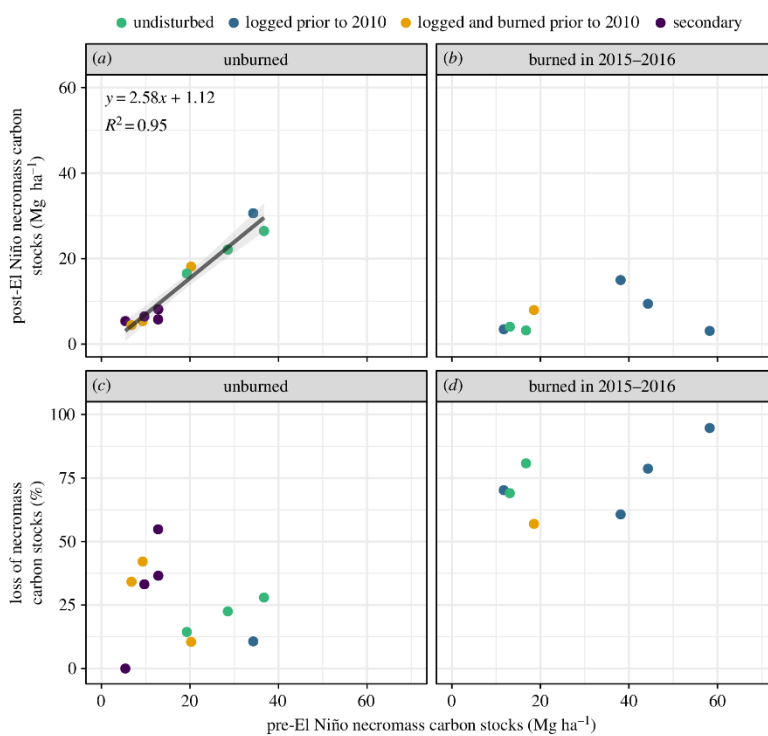

Figure 4. Pre- versus post-El Niño necromass carbon stocks in unburned control sites (*a*) and sites burned in 2015–2016 (*b*), and pre-El Niño necromass carbon stocks versus post-El Niño necromass losses in unburned control sites (*c*) and sites burned in 2015–2016 (*d*) in human-modified Amazonian forests. In panel (*a*) the black line shows the significant ($p < 0.001$) relationship between pre- and post-El Niño necromass carbon stocks in unburned sites. The equation for this relationship is shown in the panel. The grey band represents 1 s.e.m. Note that, owing to data limitations, pre- and post-El Niño necromass totals are based on CWD, FWD and leaf litter only (i.e. dead-standing stems are not included).
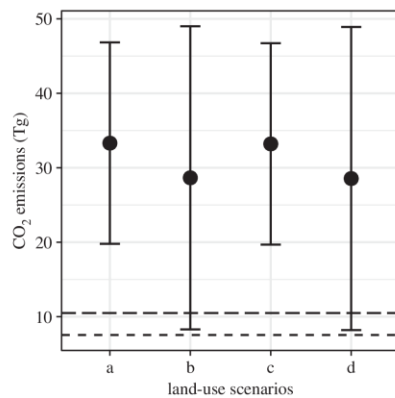
Kieran Daniel Withey - March 2019

Figure 5. Immediate CO_2 emissions for wildfires in central-eastern Amazonian human-modified tropical forests. Points show expected emissions for four land-use scenarios (see §2e and electronic supplementary material, table S1): (a) prim1 + sec1; (b) prim2 + sec1; (c) prim1 + sec2; (d) prim2 + sec2. Error bars show 95% confidence intervals. Also shown are cumulative CO_2 emissions for our study region and period from GFED 4.1s (short-dashed line) and GFAS version 1.1 (long-dashed line).

land-use scenarios (figure 5). However, the 95% confidence interval was substantially wider with land-use scenario prim2 (scenarios b and d; figure 5) owing to greater uncertainty in decomposition rates when restricted to disturbed primary forest only compared with all primary forests—undisturbed and disturbed—combined.

(d) Comparing our results with global fire emission databases

Both GFED and GFAS vastly underestimated expected wildfire CO_2 emissions for our study region and period. Respectively, these databases suggest cumulative emissions that are 77% and 68% lower than the expected value we found with land-use scenario a (prim1 + sec1; figure 5). These discrepancies can be explained by the underdetection of understorey wildfires by both GFED and GFAS algorithms. This can be seen across our whole study region but is particularly evident in areas free from historic deforestation (figure 6). GFED and GFAS appeared to be more successful at detecting fires in agricultural areas with lower levels of forest cover (figure 6). Highlighting the insensitivity of GFED to understory wildfires, this database suggests that, at most, 6% of any given $0.25°$ cell across our study region, and approximately 90 000 ha in total, burned during the 2015–2016 El Niño (figure 6e). By contrast, we show that as much as 74% of a cell (figure 6f) and almost 1 Mha of forest was affected by understory wildfires.

4. Discussion

(a) Region-wide carbon emissions from El Niño-mediated wildfires

We investigated necromass carbon stocks in human-modified forests before and after large-scale understorey wildfires in central-eastern Amazonia that occurred during the 2015–2016 El Niño. Our novel assessment revealed that expected immediate

necromass CO_2 emissions from these wildfires are around 30 Tg (figure 5). This is equivalent to total CO_2 emissions from fossil fuel combustion and the production of cement in Denmark, or 6% of such emissions from Brazil, in 2014 [46]. Consequently, wildfire-mediated immediate carbon emissions, which are not currently considered under national greenhouse gas inventories [47], represent a large source of CO_2 emissions. Moreover, these immediate emissions will be greatly exacerbated by further committed emissions resulting from tree mortality, which can be as high as 50% [16] and may not be balanced by post-fire regrowth on decadal time scales [22].

Our results add to work on prescribed burns associated with deforestation [36], contributing important information about the role of El Niño-mediated wildfires. The scale of the immediate emissions we estimated, coupled with future committed emissions, make wildfires particularly relevant to climate change mitigation programmes such as REDD+ [9,48]. For REDD+ to succeed in Amazonia, we demonstrate that forests must be protected from wildfires, as even the immediate emissions from large-scale wildfires can equal those from whole countries. Future climate change will make this only more imperative, with extreme droughts, higher temperatures, and reduced rainfall all predicted for the Amazon basin in the near future [49–51]. Wildfires may also undermine the important role that protected areas have historically served as carbon stores [52], as illustrated by the large areas burned in the Tapajós National Forest and the Tapajós-Arapiuns Extractive Reserve (figure 1).

(b) Fuel loads in humid tropical forests

Total necromass carbon stocks in the 107 RAS plots surveyed in 2010 did not vary significantly between disturbed and undisturbed primary forests (figure 2e). The mean value we found for total necromass carbon stocks in undisturbed forests was 30.2 ± 2.1 Mg ha^{-1}. This value is broadly consistent with previous estimates for the eastern Amazon. For example, Keller *et al.* [30] and Palace *et al.* [31] found necromass carbon stocks of, respectively, 25.4 and 29.2 Mg ha^{-1} in undisturbed primary forests in the Tapajós region of Pará. In primary forests disturbed by reduced-impact logging, these studies found, respectively, 36.4 and 42.75 Mg ha^{-1} of necromass carbon. However, our estimates for necromass stocks in disturbed primary forests are markedly lower (figure 2e). This discrepancy is likely a function of time since disturbance. Keller *et al.* [30] and Palace *et al.* [31] assessed necromass carbon stocks soon after disturbance, when necromass stocks are likely to be higher. By contrast, disturbance of RAS sites occurred between 1.5 and 25 years before the 2010 surveys. Necromass stocks can be highly dynamic, with residence times for most CWD estimated at less than a decade [28], especially in the case of small diameter and low wood density tree species [53]. Thus, necromass stocks in many of our disturbed primary forest sites may have had time to decrease to an equilibrium level, similar to that of undisturbed forests, where input and decomposition are largely balanced.

We did, however, find significantly larger necromass stocks in primary forests compared with secondary forests. This may be explained by (a) pre-abandonment secondary forest land-uses removing all fallen biomass with machinery or intensive fires; (b) the smaller necromass input pool in secondary forests owing to lower levels of aboveground live biomass [37]; and
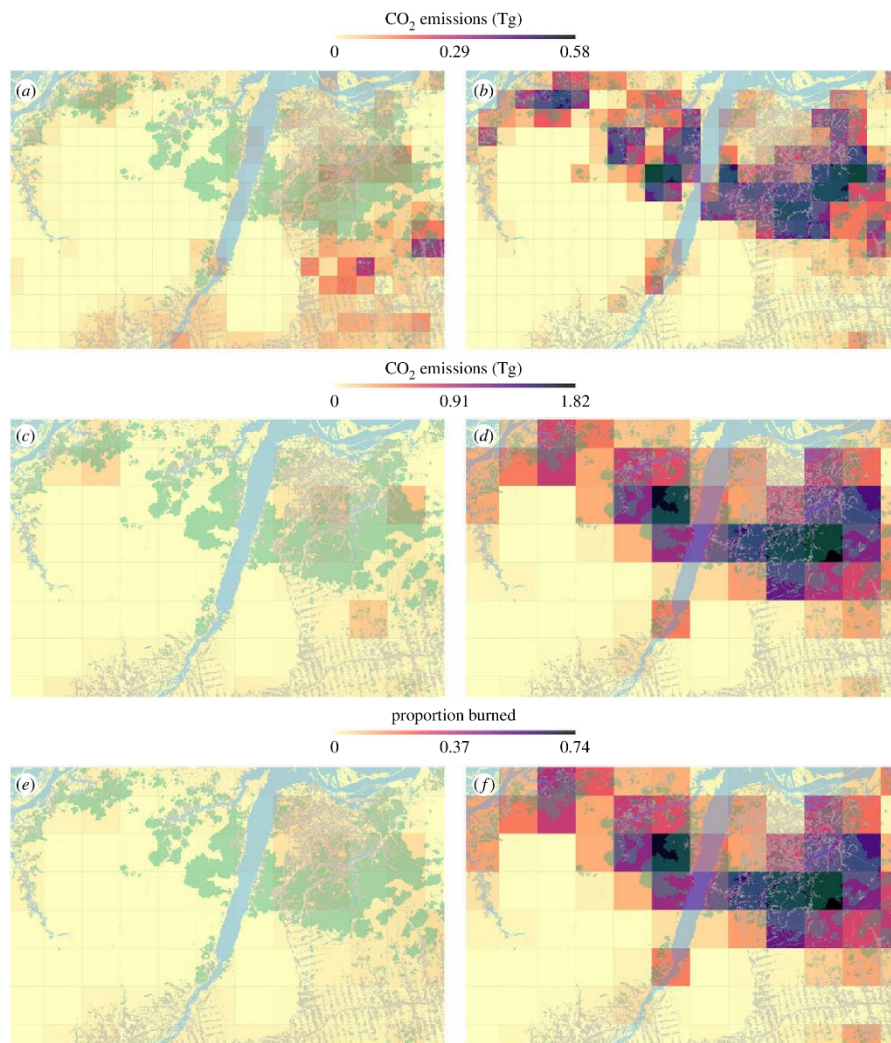
7

Figure 6. Comparing our findings with those from GFAS and GFED. CO_2 emissions for our study region and period from GFAS (*a*) and our emissions shown at the same scale (0.1°; (*b*)). CO_2 emissions from GFED (*c*) and our emissions shown at the same scale (0.25°; (*d*)). The proportion of land burned for our study region and period from GFED (*e*) and our estimate of burned area shown at the same scale (0.25°; (*f*)). In all panels, our Landsat-derived fire map is shown in dark green, deforestation in light grey and water in blue.

(c) the lower wood density of stems in secondary forests [54], resulting in more rapid CWD decomposition.

(c) Impacts of El Niño-mediated wildfires on necromass stocks

On average, we estimate that wildfires burned $87.1 \pm 2.7\%$ of our fire-affected necromass monitoring plots (figure 3*b*). This figure is substantially higher than the 62–75% burn coverage measured during experimental fires in previously undisturbed transitional Amazonian forests [18]. The areal extent of these wildfires reduced necromass (in CWD, FWD and leaf litter) carbon stocks by $46.9 \pm 6.9\%$, when gross necromass loss $(73.0 \pm 4.9\%)$ was corrected for decomposition $(26.1 \pm 4.8\%)$. The understorey wildfires that affected our burned plots were relatively low intensity, with maximum median char height of 20.5 cm. Nonetheless, our findings demonstrate that these low-intensity wildfires can dramatically diminish necromass stocks in human-modified tropical forests.

Further, both area of plot burned and necromass carbon stock losses showed little variation across disturbance classes. This may indicate that the 2015–2016 El Niño, which was

one of the strongest in recorded history, produced drought conditions so severe that necromass moisture content was reduced across all forest classes to a level that permitted combustion and sustained fires, overriding any pre-existing microclimatic differences that may have existed owing to the initial disturbance. This is further corroborated by the fact that wildfires did not distinguish between largely undisturbed forests (mostly inside protected areas) and those that have been modified by humans (mostly outside protected areas), burning vast areas of both types of forest (figure 1).

(d) Caveats

Though our dataset is the first to our knowledge that allows for quantification of necromass carbon stocks pre- and post-uncontrolled understorey wildfires in human-modified Amazonian forests, our sample size was limited, with just 18 necromass monitoring plots, of which seven burned during the 2015–2016 El Niño. Consequently, results that follow from these samples should be treated with a degree of caution. In particular, we found that necromass stock losses were not significantly related to our plot-level estimate of burned area and that fire susceptibility did not appear to vary across disturbance classes. In both cases, the lack of significance may reflect the small sample sizes rather than a genuine lack of relationship.

Moreover, owing to the limitations of our data, we assumed 100% combustion of leaf litter and FWD in the fraction of plots that burned when calculating necromass carbon losses (equation (2.1)). In a recent review, Van Leeuwen *et al.* [36] found that mean combustion completeness of leaves, litter and smaller classes of woody debris was 73–94%. However, as they acknowledge, combustion completeness can be significantly higher during El Niño years. Thus, given the strength of the 2015–2016 El Niño, and our personal observations (electronic supplementary material, figure S1), our combustion completeness assumption is likely to be reasonable.

Because of our small sample size, the 95% confidence intervals for our region-wide CO_2 immediate emissions were wide, ranging from around 8 Tg to almost 48 Tg. Future research efforts should prioritize necromass monitoring in a larger number of sites, across a range of tropical forests, to better constrain these values; as we show, such emissions have the potential to significantly exacerbate global climate change.

Despite the above limitations, there are reasons to suspect that our necromass stock loss and carbon emission estimates are highly conservative. First, we did not measure wildfire-induced carbon changes in the soil organic layer, yet research from the same region suggests that wildfires significantly reduce soil carbon pools [55]; nor could we estimate combustion of dead-standing stems, which accounted for approximately 15% of total necromass (figure 2). Second, none of the disturbed primary forest plots in which we monitored necromass changes was recently disturbed prior to the 2015–2016 wildfires, allowing time for decomposition to reduce high levels of post-disturbance necromass. Had our sample included recently disturbed sites, necromass losses would have been greater. Third, detection of low-intensity understorey wildfires continues to present a remote sensing challenge. Although manual correction of our unsupervised land-use classifications revealed only a small number of misclassifications, it is possible that some wildfire-affected sites were missed, leading to an underestimation of regional emissions.

In addition to showing that wildfire carbon emissions can be substantial, we also showed that such emissions remain poorly quantified. GFED and GFAS, CO_2 emission databases that are widely used in Earth Systems models and carbon budgets, returned considerably lower emission estimates for our study region and period than our expected values (figure 5). Nevertheless, the scale of this discrepancy is underestimated for several reasons. First, we focused solely on necromass carbon losses from understory wildfires, whereas GFED and GFAS include emissions from all land-use classes combined. Both databases therefore account for grassland and agricultural fires, which can affect large areas of human-modified tropical landscapes. Second, GFED includes both committed and immediate CO_2 emissions. Third, and again with respect to GFED, fuel loads are much high than those present in our post-disturbance plots, because they are primarily derived from slash-and-burn and deforestation studies.

(e) Conclusion

We demonstrate that there was a substantial loss of necromass following El Niño-mediated wildfires in the central-eastern Amazon. We conservatively estimate that wildfires in this region burned 982 276 ha (15.2% of our study region) of primary and secondary forest, resulting in expected immediate CO_2 emissions of approximately 30 Tg. Better understanding this large and poorly quantified source of atmospheric carbon is crucial for climate change mitigation efforts.

References

1. Wang W *et al.* 2013 Variations in atmospheric CO_2 growth rates coupled with tropical temperature. *Proc. Natl Acad. Sci. USA* **110**, 13 061–13 066. (doi:10.1073/pnas.1219683110)

2. Betts RA, Jones CD, Knight JR, Keeling RF, Kennedy JJ. 2016 El Niño and a record CO_2 rise. *Nat. Clim. Change* **6**, 806–810. (doi:10.1038/nclimate3063)

3. Zeng N, Qian H, Roedenbeck C, Heimann M. 2005 Impact of 1998–2002 midlatitude drought and warming on terrestrial ecosystem and the global carbon cycle. *Geophys. Res. Lett.* **32**. (doi:10.1029/2005GL024607)

4. Wang J, Zeng N, Wang M, Jiang F, Wang H, Jiang Z. 2018 Contrasting terrestrial carbon cycle responses to the 1997/98 and 2015/16 extreme El Niño events. *Earth Syst. Dyn.* **95194**, 1–14. (doi:10.5194/esd-9-1-2018)

5. Fanin T, Van Der Werf GR. 2015 Relationships between burned area, forest cover loss, and land cover change in the Brazilian Amazon based on satellite data. *Biogeosciences* **12**, 6033–6043. (doi:10.5194/bg-12-6033-2015)

6. Andela N *et al.* 2017 A human-driven decline in global burned area. *Science* **356**, 1356–1362. (doi:10.1126/science.aal4108)

7. Arora VK, Melton JR. 2018 Reduction in global area burned and wildfire emissions since 1930s enhances carbon uptake by land. *Nat. Commun.* **9**, 1326. (doi:10.1038/s41467-018-03838-0)

8. Hardesty J, Myers R, Fulks W. 2005 Fire, ecosystems, and people: a preliminary assessment of fire as a global conservation issue. *George Wright Forum* **22**, 78–87. (doi:10.2307/43597968)

9. Aragão LEOC, Shimabukuro YE. 2010 The incidence of fire in Amazonian forests with implications for REDD. *Science* **328**, 1275–1278. (doi:10.1126/science.1186925)

10. Aragão LEOC *et al.* 2018 21st Century drought-related fires counteract the decline of Amazon deforestation carbon emissions. *Nat. Commun.* **9**, 536. (doi:10.1038/s41467-017-02771-y)

11. van Marle MJE, Field RD, van der Werf GR, Estrada de Wagt IA, Houghton RA, Rizzo LV, Artaxo P, Tsigaridis K. 2017 Fire and deforestation dynamics in Amazonia (1973–2014). *Global Biogeochem. Cycles* **31**, 24–38. (doi:10.1002/2016GB005445)

12. Jolly WM, Cochrane MA, Freeborn PH, Holden ZA, Brown TJ, Williamson GJ, Bowman DMJS. 2015 Climate-induced variations in global wildfire danger from 1979 to 2013. *Nat. Commun.* **6**, 7537. (doi:10.1038/ncomms8537)

13. Pivello VR. 2011 The use of fire in the Cerrado and Amazonian rainforests of Brazil: past and present. *Fire Ecol.* **7**, 24–39. (doi:10.4996/fireecology.0701024)

14. Chen Y, Randerson JT, Morton DC, DeFries RS, Collatz GJ, Kasibhatla PS, Giglio L, Jin Y, Marlier ME. 2011 Forecasting fire season severity in South America using sea surface temperature anomalies. *Science* **334**, 787–791. (doi:10.1126/science.1209472)

15. Brando PM *et al.* 2014 Abrupt increases in Amazonian tree mortality due to drought–fire interactions. *Proc. Natl Acad. Sci. USA* **111**, 6347–6352. (doi:10.1073/pnas.1305499111)

16. Barlow J, Peres CA, Lagan BO, Haugaasen T. 2003 Large tree mortality and the decline of forest biomass following Amazonian wildfires. *Ecol. Lett.* **6**, 6–8. (doi:10.1046/j.1461-0248.2003.00394.x)

17. Barlow J, Peres CA. 2004 Ecological responses to El Niño-induced surface fires in central Brazilian Amazonia: management implications for flammable tropical forests. *Phil. Trans. R. Soc. Lond. B* **359**, 367–380. (doi:10.1098/rstb.2003.1423)

18. Brando PM, Oliveira-Santos C, Rocha W, Cury R, Coe MT. 2016 Effects of experimental fuel additions on fire intensity and severity: unexpected carbon resilience of a neotropical forest. *Glob. Change Biol.* **22**, 2516–2525. (doi:10.1111/gcb.13172)

19. Cochrane MA, Schulze MD. 1999 Fire as a recurrent event in tropical forests of the eastern Amazon: effects on forest structure, biomass, and species composition. *Biotropica* **31**, 2–16. (doi:10.1111/j.1744-7429.1999.tb00112.x)

20. Alencar A, Asner GP, Knapp D, Zarin D. 2011 Temporal variability of forest fires in eastern Amazonia. *Ecol. Appl.* **21**, 2397–2412. (doi:10.1890/10-1168.1)

21. Cochrane MA, Alencar A, Schulze MD, Souza CM, Nepstad DC, Lefebvre P, Davidson EA. 1999 Positive feedbacks in the fire dynamic of closed canopy tropical forests. *Science* **284**, 1832–1835. (doi:10.1126/science.284.5421.1832)

22. Silva CVJ *et al.* 2018 Drought-induced Amazonian wildfires instigate a decadal-scale disruption of forest carbon dynamics. *Phil. Trans. R. Soc. B* **373**, 20180043. (doi:10.1098/rstb.2018.0043)

23. van der Laan-Luijkx IT *et al.* 2015 Response of the Amazon carbon balance to the 2010 drought derived with CarbonTracker South America. *Global Biogeochem. Cycles* **29**, 1092–1108. (doi:10.1002/2014GB005082)

24. Liu J *et al.* 2017 Contrasting carbon cycle responses of the tropical continents to the 2015–2016 El Niño. *Science* **358**, eaam5690. (doi:10.1126/science.aam5690)

25. Gatti LV *et al.* 2014 Drought sensitivity of Amazonian carbon balance revealed by atmospheric measurements. *Nature* **506**, 76–80. (doi:10.1038/nature12957)

26. Pan Y *et al.* 2011 A large and persistent carbon sink in the world's forests. *Science* **333**, 988–993. (doi:10.1126/science.1201609)

27. Chao K-J, Phillips OL, Baker TR, Peacock J, Lopez-Gonzalez G, Vásquez Martínez R, Monteagudo A, Torres-Lezama A. 2009 After trees die: quantities and determinants of necromass across Amazonia. *Biogeosciences* **6**, 1615–1626. (doi:10.5194/bg-6-1615-2009)

28. Palace M, Keller M, Hurtt G, Frolking S. 2012 A review of above ground necromass in tropical forests. In *Tropical forests* (ed. P Sudarshana), pp. 215–252. Rijeka, Croatia: InTech.

29. Ray D, Nepstad D, Moutinho P. 2005 Micrometeorological and canopy controls of fire susceptibility in a forested Amazon landscape. *Ecol. Appl.* **15**, 1664–1678. (doi:10.1890/05-0404)

30. Keller M, Palace M, Asner GP, Pereira R, Silva JNM. 2004 Coarse woody debris in undisturbed and logged forests in the eastern Brazilian Amazon. *Glob. Chang. Biol.* **10**, 784–795. (doi:10.1111/j.1529-8817.2003.00770.x)

31. Palace M, Keller M, Asner GP, Silva JNM, Passos C. 2007 Necromass in undisturbed and logged forests in the Brazilian Amazon. *For. Ecol. Manage.* **238**, 309–318. (doi:10.1016/j.foreco.2006.10.026)

32. Keenan RJ, Reams GA, Achard F, de Freitas JV, Grainger A, Lindquist E. 2015 Dynamics of global forest area: Results from the FAO Global Forest Resources Assessment 2015. *For. Ecol. Manage.* **352**, 9–20. (doi:10.1016/j.foreco.2015.06.014)

33. Cochrane MA. 2003 Fire science for rainforests. *Nature* **421**, 913–919. (doi:10.1038/nature01437)

34. Uhl C, Kauffman JB. 1990 Deforestation, fire susceptibility, and potential tree responses to fire in the eastern Amazon. *Ecology* **71**, 437–449. (doi:10.2307/1940299)

35. Alencar A, Nepstad D, Del Carmen Vera Diaz M. 2006 Forest understory fire in the Brazilian Amazon in ENSO and non-ENSO years: area burned and committed carbon emissions. *Earth Interact.* **10**, 1–7. (doi:10.1175/EI150.1)

36. Van Leeuwen TT *et al.* 2014 Biomass burning fuel consumption rates: a field measurement database. *Biogeosciences* **11**, 7305–7329. (doi:10.5194/bg-11-7305-2014)

37. Berenguer E *et al.* 2014 A large-scale field assessment of carbon stocks in human-modified tropical forests. *Glob. Change Biol.* **20**, 3713–3726. (doi:10.1111/gcb.12627)

38. Gardner TA *et al.* 2013 A social and ecological assessment of tropical land uses at multiple scales: the Sustainable Amazon Network. *Phil. Trans. R. Soc. B* **368**, 20120166. (doi:10.1098/rstb.2012.0166)

39. Hughes RF, Kauffman JB, Jaramillo VJ. 1999 Biomass, carbon, and nutrient dynamics of secondary forests in a humid tropical region of México. *Ecology* **80**, 1892–1907. (doi:10.1890/0012-9658(1999)080[1892:BCANDO]2.0.CO;2)

40. Cummings DL, Boone Kauffman J, Perry DA, Flint Hughes R. 2002 Aboveground biomass and structure of rainforests in the southwestern Brazilian Amazon. *For. Ecol. Manage.* **163**, 293–307. (doi:10.1016/S0378-1127(01)00587-4)

41. Eggleston HS, Intergovernmental Panel on Climate Change, National Greenhouse Gas Inventories Programme 2006 *2006 IPCC guidelines for national greenhouse gas inventories* (ed. C Kankyō, S Kenkyū, L Kikan, K Miwa). Kanagawa, Japan: Institute for Global Environmental Strategies.

10

Kieran Daniel Withey - March 2019

See http://www.sidalc.net/cgi-bin/wxis.exe/ ?IsisScript=earth. xis&method=post&formato=2&cantidad=1 &expresion=mfn=001720.

42. Marthews TR *et al*. 2014 *Measuring tropical forest carbon allocation and cycling: a RAINFOR-GEM field manual for intensive census plots* (*v3.0*). Global Ecosystems Monitoring Network. See http://gem. tropicalforests.ox.ac.uk/.

43. Akagi SK, Yokelson RJ, Wiedinmyer C, Alvarado MJ, Reid JS, Karl T, Crounse JD, Wennberg PO. 2011 Emission factors for open and domestic biomass burning for use in atmospheric models. *Atmos. Chem. Phys*. **11**, 4039 – 4072. (doi:10.5194/acp-11-4039-2011)

44. van der Werf GR *et al*. 2017 Global fire emissions estimates during 1997 – 2016. *Earth Syst. Sci. Data* **9**, 697 – 720. (doi:10.5194/ essd-9-697-2017)

45. Kaiser JW *et al*. 2012 Biomass burning emissions estimated with a global fire assimilation system based on observed fire radiative power.

Biogeosciences **9**, 527 – 554. (doi:10.5194/bg-9-527-2012)

46. World Bank. 2018 CO_2 emissions. See https://data. worldbank.org/indicator/EN.ATM.CO2E. KT?view=chart (accessed 27 April 2018).

47. Bustamante MMC *et al*. 2016 Toward an integrated monitoring framework to assess the effects of tropical forest degradation and recovery on carbon stocks and biodiversity. *Glob. Change Biol*. **22**, 92 – 109. (doi:10.1111/gcb.13087)

48. Barlow J *et al*. 2012 The critical importance of considering fire in REDD+ programs. *Biol. Conserv*. **154**, 1 – 8. (doi:10.1016/J.BIOCON.2012.03.034)

49. Dai A. 2013 Increasing drought under global warming in observations and models. *Nat. Clim. Change* **3**, 52 – 58. (doi:10.1038/nclimate1633)

50. Malhi Y, Roberts JT, Betts RA, Killeen TJ, Li W, Nobre CA. 2008 Climate change, deforestation, and the fate of the Amazon. *Science* **319**, 169 – 172. (doi:10. 1126/science.1146961)

51. Spracklen DV, Garcia-Carreras L. 2015 The impact of Amazonian deforestation on Amazon basin rainfall.

Geophys. Res. Lett. **42**, 9546 – 9552. (doi:10.1002/ 2015GL066063)

52. Soares-Filho B *et al*. 2010 Role of Brazilian Amazon protected areas in climate change mitigation. *Proc. Natl Acad. Sci. USA* **107**, 10 821 – 10 826. (doi:10. 1073/pnas.0913048107)

53. Chambers JQ, Higuchi N, Schimel JP, Ferreira LV, Melack JM. 2000 Decomposition and carbon cycling of dead trees in tropical forests of the central Amazon. *Oecologia* **122**, 380 – 388. (doi:10.1007/ s004420050044)

54. Berenguer E, Gardner TA, Ferreira J, Aragão LEOC, Mac Nally R, Thomson JR, Vieira ICG, Barlow J. In press. Seeing the woods through the saplings: using wood density to assess the recovery of human-modified Amazonian forests. *J. Ecol*. (doi:10.1111/ 1365-2745.12991)

55. Durigan MR *et al*. 2017 Soil organic matter responses to anthropogenic forest disturbance and land use change in the eastern Brazilian Amazon. *Sustainability* **9**, 379. (doi:10.3390/ su9030379)

11